Influence of Seed Particle Material, Preparation, and Dynamics on Nanowire Growth

Hillerich, Karla

2013

Influence of Seed Particle Material, Preparation, and Dynamics on Nanowire Growth

Karla Hillerich

Doctoral thesis
2013

LUND
UNIVERSITY

Division of Solid State Physics
Department of Physics
Lund University

Academic Dissertation which, by due permission of the Faculty of Engineering at Lund University, will be publicly defended on Friday, February 15th, 2013 at 14:00 in Rydbergsalen, Sölvegatan 14, Lund for the degree of Doctor of Philosophy in Engineering.

Organization LUND UNIVERSITY	Document name DOCTORAL DISSERTATION
	Date of issue 2012-01-07
Author(s) Karla Hillerich	Sponsoring organization

Title and subtitle
Influence of Seed Particle Material, Preparation, and Dynamics on Nanowire Growth

Abstract

Semiconducting nanowires have attracted scientific attention for more than 20 years due to their potential applications in electronic devices, as sensors, and in solid state lighting. These applications require high quality nanowires to begin with. Achieving such good control over the growth of nanowires is not trivial and requires profound understanding of the underlying processes.

In this thesis, nanowires of different materials and combinations thereof have been grown with the help of seed particles by metal-organic vapor phase epitaxy (MOVPE). The focus of the investigations lies on the influence of several seed particle properties on nanowire growth.

First, we compared six particle preparation and deposition methods for the most common seed particle material – gold- and their influence on the growth of GaAs nanowires. We observed only small differences, mainly in incubation times, which did not have a significant effect on the nanowire length after some growth time, though. The optical properties, however, varied between nanowires seeded by different particle types.

Further, copper as seed particle material for growth of InP nanowires and InP-InAs heterostructures was investigated. The aim was to get a deeper understanding of which properties or combination of properties determine a "good" seed particle material. InP nanowire growth from Cu particles differs a lot from nanowire growth from Au seed particles in terms of temperature range and precursor molar fractions. Furthermore, growth from two types of particles – Cu-rich and In-rich – occurs simultaneously at low V/III ratios. The investigations of InP-InAs heterostructures showed that it is indeed possible to grow straight heterostructures, but we observed unusual layer formation of the InAs segments.

Finally, we used the possibility of *in situ* TEM to investigate nanowire growth at the IBM T.J. Watson Research Center. We combined group IV and group III/V materials and investigated the particle dynamics that may lead to kinking. In addition, we investigated the instantaneous kinetics of GaP growth.

Key words
III-V seminconductor materials, nanowires, metal-organic vapor phase epitaxy, *in situ* TEM

Classification system and/or index terms (if any)

Supplementary bibliographical information	Language English
ISSN and key title	ISBN 978-91-7473-449-2
Recipient´s notes	Number of pages 147 / Price
	Security classification

Distribution by (name and address)

Influence of Seed Particle Material, Preparation, and Dynamics on Nanowire Growth

Karla Hillerich

Doctoral thesis
2013

LUND
UNIVERSITY

Division of Solid State Physics
Department of Physics
Lund University

Division of Solid State Physics
Department of Physics
Lund University
22100 Lund
Sweden

ISBN 978-91-7473-449-2
Printed in Sweden by Media-Tryck, Lund University
Lund 2013

Table of Content

Abstract

Semiconducting nanowires have attracted scientific attention for more than 20 years due to their potential applications in electronic devices, as sensors, and in solid state lighting. These applications require high quality nanowires to begin with. Achieving such good control over the growth of nanowires is not trivial and requires profound understanding of the underlying processes.

In this thesis, nanowires of different materials and combinations thereof have been grown with the help of seed particles by metal-organic vapor phase epitaxy (MOVPE). The focus of the investigations lies on the influence of several seed particle properties on nanowire growth.

First, we compared six particle preparation and deposition methods for the most common seed particle material – gold - and their influence on the growth of GaAs nanowires. We observed only small differences, mainly in incubation times, which did not have a significant effect on the nanowire length after some growth time, though. The optical properties, however, varied between nanowires seeded by different particle types.

Further, copper as seed particle material for growth of InP nanowires and InP-InAs heterostructures was investigated. The aim was to get a deeper understanding of which properties or combination of properties determine a "good" seed particle material. InP nanowire growth from Cu particles differs a lot from nanowire growth from Au seed particles in terms of temperature range and precursor molar fractions. Furthermore, growth from two types of particles – Cu-rich and In-rich – occurs simultaneously at low V/III ratios. The investigations of InP-InAs heterostructures showed that it is indeed possible to grow straight heterostructures, but we observed unusual layer formation of the InAs segments.

Finally, we used the possibility of *in situ* TEM to investigate nanowire growth at the IBM T.J. Watson Research Center. We combined group IV and group III/V materials and investigated the particle dynamics that may lead to kinking. In addition, we investigated the instantaneous kinetics of GaP growth.

Populärvetenskaplig Sammanfattning

Många material är kristallina – inte bara ädelstenar, utan även alla metaller och keramiska material består av kristaller. Till och med många proteiner och t.ex. acetylsalicylsyra, basen till aspirin, bildar kristaller. När någonting kallas kristallint menar man att atomerna sitter på särskilda platser och i en bestämd, regelbunden ordning. De flesta material är polykristallina, vilket betyder att de består av många små kristaller. Däremot är det inte så enkelt att producera enkristallina material, d.v.s. en hel bit som bara består av en kristall. I vår forskning bedriver vi växt av enkristaller – väldigt små enkristaller. De är endast några tiotals nanometer tjocka och några mikrometer långa och de brukar kallas nanotrådar. En mikrometer är en tusendel av en millimeter och en nanometer är i sin tur en tusendel av en mikrometer.

Kristallerna vi producerar består av halvledande material. Ett halvledande material är ett ämne som bara leder ström under speciella förutsättningar. Laddningsbärarna, det vill säga elektronerna, kan inte passera ett energetiskt förbjudet område placerat mellan två tillståndsområden som är energetiskt tillåtna. I halvledare kan man ändra materialets egenskaper genom dopning, vilket innebär att man tillsätter (eller tar bort) elektroner. På det viset kan fler elektroner finnas tillgängliga för att t.ex. leda ström.

När kristaller är tillräckligt små påverkar deras storlek elektronernas rörlighet. I de nanotrådar som vi jobbar med begränsas rörligheten i två dimensioner och bara i en dimension kan elektronerna flytta sig helt fritt. Att nanotrådarna är så små gör också att man kan kombinera olika material på ett bättre sätt än i mer storskaliga strukturer. Man har visat att det är möjligt att bygga transistorer, solceller och även lysdioder (LEDs) av nanotrådar.

Hur växten av nanotråder fungerar och hur man kan kontrollera den står i fokus i denna avhandling. Nanotrådar växer på ett underlag, ett så kallat substrat. På grund av kristallordningen växer de i lodrät riktning i förhållande till substratets yta. För att få nanotrådar i stället för en stor kristall måste man se till att växten är snabbare på höjden än vad den är på bredden. Detta går att göra genom att man använder sig av så kallade odlingspartiklar. Atomerna som anländer till substratet stannar hellre vid en sådan partikel än någon annanstans på substratet. I partikeln stiger koncentration av ankommande atomer och partikeln övermättas efter en stund, vilket betyder att koncentrationen är högre än jämviktskoncentration, och material måste fällas ut. Då bildas en enkristall under partikeln och nanotråden växer fram samtidigt som den lyfter partikeln.

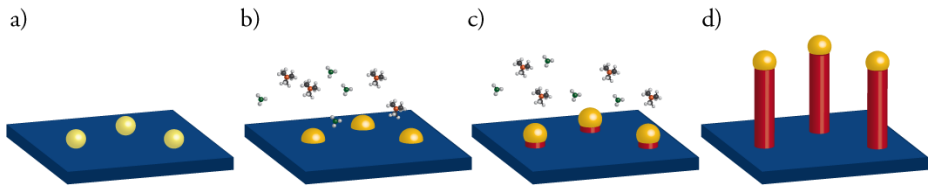

Figure 1: Schema av nanotrådsväxt. *a) Odlingspartiklar placerat på substratet, b) Atomerna kommer in och fastnar i partiklarna c) Partiklarna övermättas, nanotrådar börja växa och lyfter partiklar up d) efter en visst längd slutar man nanotrådsväxten*

Sådana enkristallina trådar har man låtit växa med hjälp av metallpartiklar i många decennier (i storleksordningen nanometer i ungefär 20 år). Det vanligaste partikelmaterialet som används är guld. Guldpartiklar fungerar väldigt bra som odlingspartiklar av många olika skäl. Vi har ännu inte fullt ut förstått varför guld fungerar så bra, och exakt vad som behövs för att ett material ska lämpa sig som ett bra odligsämne är heller inte känt. En viktig fråga som jag försöker besvara i detta arbete är hur odlingspartikeln måste vara beskaffad för att fungera optimalt.

En del av mitt arbete har ängnats åt hur olika framställningsmetoder av guldpartiklarna påverkar nanotrådsväxten och deras egenskaper. Vi såg att det finns små skillnader i början av växten p.g.a. olika föroreningar, men i stort sett växer nanotrådarna lika bra från alla typer av guldpartiklar som vi jämförde. Vi fastställde dock att nanotrådarnas optiska egenskaper, d.v.s. hur de lyser när man utsätter dem för en elektronstråle, var ganska olika, beroende hur man hade framställt partiklarna.

Vi jämförde inte bara guldpartiklar med lite olika egenskaper utan bytte även material till koppar. Det är inte bara intresset av att förstå tillväxtprocessen utan även nödvändigten från ett industriellt perspektiv som driver forskningen till att ersätta guld. Guldet kan nämligen förstöra halvledarens egenskaper. Resultaten visar att det finns en stor skillnad mellan nanotrådsväxt från guld och från koppar. Det verkar som att kopparpartikeln på nanotråden ändrar sitt tillstånd flera gånger under växten, vilket leder till stora instabiliteter. I sådana fall kan man bara spekulera i vad som händer, eftersom vi bara kan titta på proverna efteråt. Tänk om man skulle kunna kika in i växtreaktorn...Våra samarbetspartners från IBM har sådana möjligheter. De har ett mikroskop som tål att man har gas i kammaren samtidigt som man tittar på något. Det betyder att vi kan titta på nanotråden medan den växer och således att vi kan observera vad som egentligen händer med partikeln under växten. Så upptäckte de t.ex. ett väldigt spännande förhållande vid gränsytan av partikeln och tråden som man inte hade kunnat föreställa sig om man inte hade sett det. På IBM har vi bland annat undersökt vad som egentligen är orsaken till att nanotrådarna ibland böjer sig när man kombinerar olika material.

List of Symbols

β	Semi-angle of collection of a lens
γ	Surface energy
γ_{AB}	Interface energy
δ	Resolution
η	Cu_2In phase
Λ_S	Surface diffusion length
λ	Wavelength
μ	Chemical potential
σ	Surface energy density
τ_s	Mean time of residence
$\chi(\mathbf{u})$	Exponential term in the aberration function
Ω	Atomic volume
a	Mean distance between adsorption sites
a_i	lattice constant
C_i	Concentration
C_S	Spherical aberration
D_s	Surface diffusion coefficient
Δf	Overfocus
Δf_{sch}	Scherzer defocus
ΔG	Gibbs free energy
E	Electron energy
E_C	Envelope function related to defocus spread
E_{des}	Activation energy for desorption
E_S	Envelope function related to illumination convergence
E_{sd}	Activation energy for surface diffusion
$F(\mathbf{u})$	Specimen function
$G(\mathbf{u})$	Area in the image
$H(\mathbf{u})$	Contrast transfer function
I_i	Intensity
j	Number of atoms in a nucleus
k	Boltzmann constant (1.38065×10^{-23} J/K)
k_{ij}	Cliff-Lorimer factor
n	Refractive index
p	Pressure
R	Gas constant (8.3145 J/mol K)
r	Radius

S	Supersaturation
T	Temperature
$\mathbf{u}$	Reciprocal lattice vector
X	Surface energy term
Z	Element mass

List of Acronyms

AEM	Analytical electron microscopy
AES	Auger electron sprectroscopy
bcc	Body-centered cubic
BF	Bright field
BSE	Backscatter electrons
CCD	Charged-coupled device
CBE	Chemical beam epitaxy
CL	Cathodoluminescence (spectroscopy)
CTEM	Conventional transmission electron microscopy
CTF	Contrast transfer function
DDC	Direct deposition of colloidal particles
DF	Dark field
DI	De-ionized water
DMA	Differential mobility analyzer
EBL	Electron-beam lithography
EBD	EBL-defined particles
ECA	Aerosol particles generated by evaporation/condensation
EELS	Electron energy loss spectroscopy
EPC	Electronic pressure controller
ESC	Electro-spray deposition of colloidal particles
ESAC	Electro-spray deposition and annealing of colloidal particles
fcc	Face-centered cubic
FFT	Fast-fourier transformation
HAADF	High-angular annular dark field
hcp	Hexagonally closed packed
HR-TEM	High-resolution transmission electron microscopy
LPE	Liquid phase epitaxy
MBE	Molecular beam epitaxy
MFC	Mass-flow controller
MO	Metal-organic
MOCVD	Metal-organic chemical vapor peposition
MOVPE	(also OMVPE) Metal-organic vapor phase epitaxy
PIN	Preferential interface nucleation
PLL	Poly-(L)-lysine
SDA	Aerosol particles generated by spark discharge
SE	Secondary electrons

SEM	Scanning electron microscopy/microscope
TBA	Tertiabutylarsine
TBP	Tertiabutylphosphine
TEG	Triethyl-galllium
TEM	Transmission electron microscopy/microscope
TMA	Trimethyl-aluminum
TMG	(or TMGa) Trimethyl-gallium
TMI	(or TMIn) Trimethyl-indium
TPB	Triple-phase-boundary
UHV	Ultra high vacuum (pressure lower than 10^{-9} mbar)
VLS	Vapor-liquid-solid
VSS	Vapor-solid-solid
WZ	Wurtzite
XEDS	X-Ray energy dispersive spectrometry
ZB	Zinc blende

List of Papers

The thesis is based on the following articles.

I. A comparative study of the effect of gold seed particle preparation method on nanowire growth
M.E. Messing, K. Hillerich, J. Bolinsson, K. Storm, J. Johansson, K.A. Dick, K. Deppert, Nano Research, 3 (2010) 506-519.

I took part in the planning of the project, conducted large parts of the characterization and analysis, and developing the article.

II. Epitaxial InP nanowire growth from Cu seed particles
K. Hillerich, M.E. Messing, L.R. Wallenberg, K. Deppert, K.A. Dick, J. Cryst. Growth, 315 (2011) 134-137.

I planned the project, conducted all experiments, their characterization, and their analysis, and I wrote the article.

III. Simultaneous growth mechanisms for Cu-seeded InP nanowires
K. Hillerich, K. Dick, M. E. Messing, K. Deppert and J. Johansson, Nano Research, 5 (2012) 297-306

I planned the project, conducted all experiments, the characterization and their analysis, and I wrote the manuscript.

IV. Strategies to control morphology in hybrid group III-V/group IV heterostructure nanowires
K. Hillerich, K. A. Dick, C.-Y. Wen, M. C. Reuter, S. Kodambaka, F M. Ross, submitted to Nano Letters

I performed growth experiments, extracted, analyzed, and interpreted data, and wrote the manuscript together with Frances Ross.

The following papers are not included in the thesis:

1. The use of gold for fabrication of nanowire structures

M.E. Messing, K. Hillerich, J. Johansson, K. Deppert, K.A. Dick, Gold Bulletin, 42 (2009) 172-181

I took part in the discussion of the concept of the article, contributed some parts of the text and illustrations and took part in the discussion of the article.

2. Growth Mechanism of Self-Catalyzed Group III-V Nanowires

B. Mandl, J. Stangl, E. Hilner, A.A. Zakharov, K. Hillerich, A.W. Dey, L. Samuelson, G. Bauer, K. Deppert, A. Mikkelsen, Nano Letters, 10 (2010) 4443-4449

I performed parts of the SEM characterization and dimension measurements. I took part in the discussion of the manuscript.

3. Periodically changing morphology of the growth interface in Si, Ge, and GaP nanowires

C.Y. Wen, J. Tersoff, K. Hillerich, M.C. Reuter, J.H. Park, S. Kodambaka, E.A. Stach, F.M. Ross, Phys. Rev. Lett., 107 (2011) 025503

I grew the GaP nanowires, took part in the *in situ* experiments on them and took part in the discussion of the manuscript.

4. A cathodoluminescence study of the influence of the seed particle preparation method on the optical properties of GaAs nanowires

A. Gustafsson, K. Hillerich, M. E. Messing, K. Storm, K. A. Dick, K. Deppert and J. Bolinsson, Nanotechnology, 23 (2012) 9.

I took part in the planning of the project, performed particle depositions and growth experiments and took part in developing the manuscript.

Acknowledgments

It would have been a waltz for me, if I had to write a thesis about all the people I met on my way. Unfortunately, I have to limit my acknowledgments to a tiny part of the thesis. Although one might think, nanowires are the main actors in the play, the people actually are! I am happy to be part of this very inspiring research group.

There are some people I am especially grateful to for their help or for just making my days:

I thank the whole Crystal Growth & Materials Science group for lively discussions, ideas and advices during our meetings. I learned a lot on Friday mornings.

I thank my supervisors Jonas Johansson, Knut Deppert, and Kimberly Dick Thelander for their support, their ideas, inspiring discussions, and comments on my work and writing.

Jonas, you help me to get structure in my chaotic thoughts. You are always so kind and supporting. You even taught me a lot of patience.

Knut, you have been such a caring supervisor, I know you are always there for me, helping in both work and private problems. When I get stuck, you also help me to find the exit.

Kimberly, thank you for convincing Jonas and Knut, that you need me here! Thank you for all your knowledge on nanowires, all the useful comments, discussions, and - last, but not least- the barbecues at your place.

I had the possibility to spend some time at the *in situ* TEM at the IBM T.J. Watson Research Center, Yorktown Heights with great scientists. This has always been a great time in the lab with Frances, Cheng-Yen, and Yi-Chia. I thank Frances' family so much for hosting me so warmly and for helping me when I was sick.

I thank the nCHREM people Gunnel, Martin, and Reine for patiently teaching me the TEM and helping me with the troubles I tend to have with the instrument.

Thank you, Magnus and Sebastian, for very useful discussions and much practical help on MOVPE and nanowire growth.

I thank Bengt for being such a great problem solver and friend. Apart from talking to you about the moods of an old lady, it is great to chat about anything else in life with you, too. Without Søren's endless source of knowledge and his work on the machine, we would not have been able to finally start it again. Thank you.

I thank Dario for helping me with tedious TEM and STEM investigations on my strange heterostructure nanowires.

The people who make our lab working so smoothly, that we can concentrate on research and we tend to only recognize them, if something doesn't work…Heiner, Lars, Anneli, Anders, Line, Mona, Mari, Monica, Ivan, Peter, Peter, Mariusz, Håkan, George, Anders, Lena, Bengt, Karin, and Elsie. Thank you for your help anytime I asked.

Supervising "my" master student Fangfang was a great experience, even though I am quite spoiled now. Fangfang, you always warm my heart with your little somethings, cakes and nice emails.

Bernhard welcomed me here, told me all important stories and made my time here much easier. I appreciate the hours of "sudern" and all the things I learned from you. Jessica, it was great working with you and thank you for all your help (and your nice figures). You see things differently and that is a great inspiration. Monica brightened every corridor and lunch room, when she still was working here. I am happy, that we still manage to meet from time to time. I thank Andreas for conversations, language corrections, apples, hugs, and more; Nicklas for entertainment late in the evenings; and Daniel for cakes, hugs, and trust. Thanks also to the "twins", Håkan and George, for my daily dose of compliments and skitsnack.

I am proud to be able to use the term "my girls" for the first time in my life. I have so much fun with you, Mia Muffin, Fia Falafel, Mercy Men-Magnet, Sofia Smultron, and Sepideh Super-Match. Our adventures are legendary. I am looking forward to more Paradises, Ginger Apple Martinis, gaggles and giggles, and cry babies.

Maria and me – the fantastic couple. Unfortunately, we didn't work together enough, the few times have been so straightforward and inspiring. But, we have such a great time together otherwise, which counts much more. Thank you for being such a great friend, always there with an ear to listen, an honest mouth to give useful advice, and an open mind to understand our somewhat different perspectives to life.

I thank all my friends in Germany, who haven't forgotten me and welcome me in the rare moments I meet them as if I have never been away. I am especially happy that many of you find the way to Lund and visit me! I am especially grateful to Annette, my sister, Tanja, Simon, Helene, Lisa, Heike, Holgi, Christian, Andi, Daniel, and Chrisje for all their support and friendship during difficult times.

I thank E. for accompanying me during the first part on my way to a PhD.

My family, who supported my curiosity and fantasy and all my way to where and who I am now. Thank you so much. Thank you that I can always count on you whatever happens. The uncountable parcels with food and precious things from the homeland made my life much nicer.

1 Introduction

The trend of miniaturization can be observed in almost all areas of technology. Examples include mobile phones, computers, medical operation tools or lab-on-a-chip applications. The reason for miniaturization lies not only within the possibility to fabricate smaller devices, but also in the fact that new effects appear as soon as the size reaches the nanometer range. One consequence of the diminutive size is the large surface-to-volume ratio of nanostructures. This increases the efficiency of catalysts or the sensitivity of sensors. Furthermore, the mechanical properties change with down scaling, since certain deformation mechanisms are no longer energetically favorable. Moreover, some material phases which do not exist in bulk are stable at small size scales. The size has even more significant effects on the electrical, optical, and magnetic properties. In this size range the carriers are confined and quantum effects play a major role.

To fabricate such nanostructures, two main fabrication concepts are applied: top-down and bottom-up. In top-down processes, the nanostructure is fabricated from a macroscopic material. A common method is lithography, where a pattern is transferred onto the material and the structures are then engraved or deposited along the pattern. The bottom-up approach uses self-organization of molecules and particles, which assemble to certain structures. Natural processes are bottom-up processes, and a lot can be learned by studying nature's way of structure formation, such as DNA, membranes and minerals. Examples of bottom-up processes are the formation of colloids, quantum dots, nanowires and biomineralization. It is often easier to control top-down approaches, but they suffer from complicated and expensive processes. In addition, it is difficult to form arbitrarily small structures. With bottom-up processes, smaller objects can be achieved in a more simple way, but finding a good way of control is typically more challenging. In practice, a combination of bottom-up and top-down techniques is often applied.

Even in crystal growth, the miniaturization trend has been followed. Crystal growth is in itself an example of a bottom-up technique, since atoms assemble into a crystal lattice. The processes in crystal growth and epitaxy (a method of crystal growth used to achieve perfect and oriented crystals) are presented in chapter 2 of this work. Besides the controlled growth of bulk crystals (3D), techniques to grow thin-films of high quality have been developed, such as liquid-phase epitaxy (LPE), molecular beam epitaxy (MBE), and VPE (vapor-phase epitaxy). Very thin layers can be obtained, leading to so-called quantum wells, where the electrons are confined in one dimension but are free in the other two (2D). By refining the fabrication techniques,

self-assembly of zero-dimensional (0D) crystals, i.e. quantum dots (in terms of the electron confinement), has been realized. These structures form due to differences in surface energy or strain. Other than 3D, 2D and 0D growth, 1D growth has been performed as well, resulting in nanowires (NWs). Nanowires can be grown horizontally on a substrate or extending out from it. We aim for nanowires which are vertically-aligned to the substrate, by using the correct crystallographic substrate orientation. Their electronic and optical properties as well as the possibility to combine materials, which cannot be combined in thin-films or quantum dots, triggers a high interest in growth of nanowires. A large number of nanowire devices have been realized, such as transistors [1, 2], light-emitting diodes [3, 4], solar cells [5] and biosensors [6].

The growth and application of nanowires is nowadays a research area with thousands of articles published per year. The growth of one-dimensional structures is well established, but has disappeared from focus for a while. The fabrication of "hairy" silver crystals by heating argentite (Ag_2S) was reported already in 1778 [7]. In the 1950s to the 1970s, intensive research on whiskers with dimensions in the range of µm to cm was undertaken. The Proceedings of the International Conference on Crystal Growth 1958 [8] solely dedicated to whiskers show this in an impressive way, with 275 pages from 24 authors. For a long time, research was more focused on metallic, oxide and carbide whiskers, and their mechanical properties. In 1964, Wagner and Ellis proposed the famous vapor-liquid-solid (VLS) mechanism for the growth of Si whiskers with the help of Au seed particles [9], which is still the basis of our work. Not much later GaAs and GaP whiskers were grown via VLS with the help of Au, Pd, Pt [10, 11] and even self-seeded with Ga [12]. However, whiskers were rather an undesirable effect in thin-film growth at that time [13]. Only a few researchers like Givarzigov continued to work on semiconductor whisker growth [14]. In 1991, Hiruma *et al.* discovered the growth of GaAs nanowhiskers in MOVPE, which were 10-20 nm wide and 1-5 µm long [15]. They first assumed a gold free growth, but admitted one year later that they had gold residues in their chamber [16]. The interest in single crystal semiconductor nanowhiskers or nanowires (the terms are synonyms) was and still is much higher than in microwhiskers, since they have these interesting properties due to 2D carrier confinement [1, 17] as mentioned before. Within the last two decades, nanowire growth of group IV materials [18-20], virtually all III/V materials [21, 22] as well as the growth of II/VI [23, 24] nanowires has been shown. The first article on nanowire growth from Lund was published as late as 2001 [25], and was followed until now by about 100 publications solely dedicated to nanowire growth. The growth of nanowires is described in detail in chapter 5. As the research group at Solid State Physics in Lund University concentrates on III/V semiconducting materials, only those will be discussed further on.

In our and many other scientific groups, particle-assisted nanowire growth on the basis on Wagner and Ellis' VLS mechanism is the dominating growth method. Although particle-assisted NW growth has been conducted for many years and there

have been great findings on the atomic and thermodynamic mechanisms behind the function of particle enhanced 1D growth, the image is not yet complete and there are several mysteries left. My research takes a close look on the particle. My contribution is mainly focused on the properties of the particles, and how they influence the NW growth. The aim of my thesis is to shed light on some aspects towards a complete understanding of the mechanism; after these five years I can see that the road is long and stony, and there are many challenges left.

One part of my research was to investigate the influence of different particle preparation methods on the growth of NWs; i.e. how different impurities or crystal structures change the properties of the gold particles concerning their ability to enable NW growth [paper I] and the optical properties of the NWs [26].

The other, main project goes one step further and changes the seed material from gold to copper. Both materials are similar, but the behavior as seed material differs remarkably [paper II,III].

An even deeper insight into the behavior of the particle was reached during the work with Dr. Frances Ross at IBM T.J. Watson Research Center, where we investigated Si and GaP nanowire growth *in situ* in a transmission electron microscope. We investigated the change of composition, diameter, and kinking in dependence of the growth conditions. We also realized multilayers of material combinations considered difficult to grow before [paper IV]. Part of our collaboration helped to establish a general observation, namely that NWs grow via an oscillating corner at the particle/NW interface (see chapter 5.1) [27]. These findings were revolutionary for the understanding of nanowire growth. Finally, we managed to grow GaP NWs *in situ*, which is unique until now. Our observations give rise to a new view on the influence of the precursors and the formation of crystal defects during growth.

This thesis is built up as follows. In chapter 2, the basic concepts of crystals and crystal growth are introduced. The experimental fabrication methods applied in this work are described in chapter 3. Chapter 4 is dedicated to electron microscopy, which is the crucial characterization technique for our research. In chapter 5, nanowire growth is discussed in detail, including my contributions to the field. Finally, I will conclude the thesis.

2 Crystals and Crystal Growth

Crystals and their growth form the core of the thesis. This chapter introduces the fundamental concepts of crystals to be known for further reading and the processes and factors which control crystal growth. It presents a special kind of crystals – semiconductors – and a special way of crystal growth – epitaxy. Finally, the reader gets a glimpse on size effects on the formation of crystals.

2.1 Crystals

Crystals can be defined as solids with ordered atomic structure in contrast to amorphous materials, where the atoms do not have a long-range order. In the crystal, atoms are situated at certain crystal lattice sites. The lattice itself consists of units of arranged atoms which are repeated by translation. These units describe the geometric relation of the atoms to each other, and are called unit cells. The simplest unit cells are simple cubic, body-centered cubic (bcc), face-centered cubic (fcc) and hexagonal closed packed (hcp) lattice (Fig. 2.1).

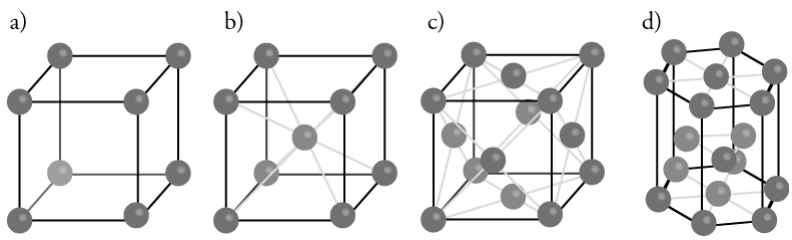

Figure 2.1: Unit cells of crystal lattices. *a) simple cubic, b) body-centered cubic, c) face-centered cubic, and d) hexagonal closed packed*

Crystals show direction dependent properties, so-called anisotropy, due to the different geometry, packing density, and relation of neighboring atoms. Anisotropy leads amongst others to different carrier mobilities, elastic properties, and growth rates in different crystallographic directions. Directions or families of planes of the same packing are identified by Miller-indices [28], three or four numbers for cubic or hexagonal systems, respectively.

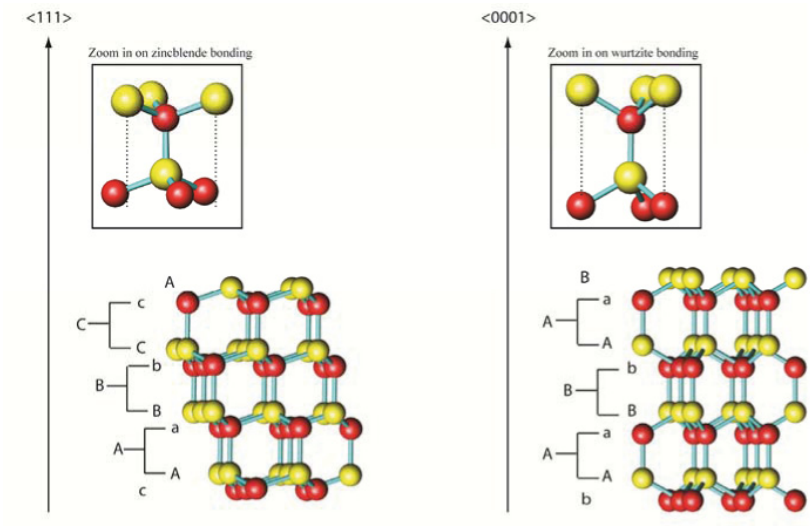

Figur 2.2: Atomic stacking of ZB (left) and WZ (right) *in <111> and <0001> direction, respectively. The two colors represent two types of atoms, group III and group V, respectivel. [Courtesy of J. Bolinsson].*

The {111} planes in the fcc system and the {0001} planes in the hcp system are the closest packed plane with every atom having six in-plane neighbors. These directions are the preferential growth directions of nanowires and therefore important for this work. These planes of hexagonally arranged atoms can be stacked in different sequences. In fcc the stacking order is ABCABCABC…, whereas in hcp, layers are stacked ABABAB…In III/V nanowires, two crystal structures form: the cubic zinc blende (ZB) and the hexagonal wurtzite (WZ) [29](Fig. 2.2). These structures can either be seen as dumbbells of a group III and a group V atom sitting on the lattice sites of fcc and hexagonal lattices, respectively, or two lattices interpenetrating each other. So, ZB and WZ are only different in their stacking. This means that a stacking fault in one or the other structure may lead to a switch between ZB and WZ. Since the stacking fault energy is not extraordinarily high [29], a mixed structure is a result in nanowires for most conditions. The exact tuning of the crystal structure in nanowires has been achieved though [29-32].

2.1.1 Semiconductors

Semiconductors are a class of materials with special electronic properties. Here, only crystalline semiconductors are introduced. Semiconductors are the basis for diodes, micro-electronic devices, transistors, solar cells, light-emitting diodes, and photo-detectors. The number of electrons of the atoms in combination with the crystallographic arrangement leads to the formation of so-called energy bands, within which the electrons can take any energy state. In semiconductors, one energy band, the valence band, is filled with electrons, the other one, the conduction band, is empty in the ground state and separated from the valence band by a zone of forbidden energy states, the band gap. In semiconductors, this gap is small enough, so that the electrons can overcome it, if they are excited by thermal energy or by an electric potential. As soon as electrons reach the conduction band, the material can conduct current. The special feature of semiconductors is, that this conductance can be controlled by the amount of free carriers. Their number can be increased, as mentioned above, by applying temperature or a voltage, as well as by inserting additional states close to the band edge, from where electrons easily can reach the band. This so-called doping is realized by addition of impurity atoms with another amount of electrons. Electrons can also be excited by light having a wavelength smaller or corresponding to the band gap. This is applied in solar cells, where electrons are excited by the sunlight to the conduction band and induce a current. Light-emitting diodes work the other way round: Electrons, which are pumped through the device, fall down from the conduction band to the valence band and emit light with a wavelength corresponding to the band gap.

2.2 Crystal Growth

Crystal growth is a self-organizing process, where atoms assemble in an ordered manner, and is driven and controlled by thermodynamics and kinetics. Here, I concentrate on crystal growth on existing crystalline surfaces, and introduce epitaxy.

2.2.1 Thermodynamic and kinetic aspects of crystal growth

Crystal growth is controlled by thermodynamics and kinetics. Thermodynamics describes the driving force for all processes: reaching thermodynamic equilibrium which is the point of lowest free energy for the system. The rates at which processes take place are described by kinetics. In many cases, thermodynamic equilibrium is never reached, since the processes occur too slowly. These processes are referred to as kinetically hindered. In other words, thermodynamics determine what happens, kinetics determine how fast it happens. The occurrence of vapor pressure, for example, is an equilibrium effect, i.e. thermodynamic, whereas crystal growth from the vapor is a typical kinetic effect [33]. It is crucial to distinguish between these two effects properly. They will be described on the following pages.

The thermodynamic approach can be used to explain a number of phenomena during growth. The driving force for a phase change is the difference in chemical potentials μ of two phases:

$$\Delta\mu = \mu_1 - \mu_2 \qquad (2.1)$$

At equilibrium, $\Delta\mu$ is zero. Let us assume phase *1* is vapor or liquid and phase *2* is solid. If $\Delta\mu > 0$, material would condensate, if $\Delta\mu < 0$, material would evaporate or dissolve/melt. The difference in chemical potential can be expressed in terms of the temperature T and the supersaturation S:

$$\Delta\mu = RT \ln S \qquad (2.2)$$

The supersaturation is the ratio between a growth promoting quantity F (during the process) and at equilibrium F_{eq}:

$$S = \frac{F}{F_{eq}} \qquad (2.3)$$

The quantity F can be pressure, concentration, molecular fluxes amongst others. In some cases $\Delta\mu$ is referred to supersaturation instead.

The classical nucleation theory gives the Gibbs free energy ΔG for nucleation of an island depending on the number of atoms j in the nucleus as follows [34]:

$$\Delta G(j) = -j\Delta\mu + j^{2/3}X \tag{2.4}$$

where X is a surface energy term:

$$X = \sum_k C_k\gamma_k + C_{AB}(\gamma_{AB} - \gamma_B) \tag{2.5}$$

The first term stands for the surface energy of the different faces of the island (C_k is a geometrical factor, depending on the shape of the island), the second term stands for the interfacial energy between materials or layers A and B; γ_{AB} is the interfacial energy of the new interface with the area C_{AB}, γ_B is the surface energy of B.

The plot of $\Delta G(j)$ vs. j (Fig. 2.3) has a maximum at the critical cluster size j^*

$$j^* = \left(\frac{2X}{3\Delta\mu}\right)^3 \tag{2.6}$$

The nucleation barrier is then given by

$$\Delta G^*\left(j^*\right) = \frac{4X^2}{27\Delta\mu^2} \tag{2.7}$$

Nucleation of a layer in nanowires can rather be treated as 2D growth [35], that is nucleation of a monolayer. The supersaturation is then in relation to the corresponding step in the adsorption isotherm [34] and expressed in terms of pressure p, i.e.

$$\Delta\mu' = RT\ln\tfrac{p}{p_{eq}} \tag{2.8}$$

and $\Delta G_{2D}(j)$ becomes then

$$\Delta G_{2D}(j) = -j\Delta\mu' + j^{1/2}X \tag{2.9}$$

The square root expression is due to the extra edge energy X.

The maximum is then at

$$j^* = \left(\frac{X}{2\Delta\mu'}\right)^2 \tag{2.10}$$

and

$$\Delta G^*_{2D}(j^*) = \frac{X^2}{4\Delta\mu'} \tag{2.11}$$

where $\Delta\mu' = \Delta\mu - \Delta\mu_c$ and $\Delta\mu_c = (\gamma_A + \gamma_{AB} - \gamma_B)\Omega^{2/3}$, Ω is the atomic volume of the deposit.

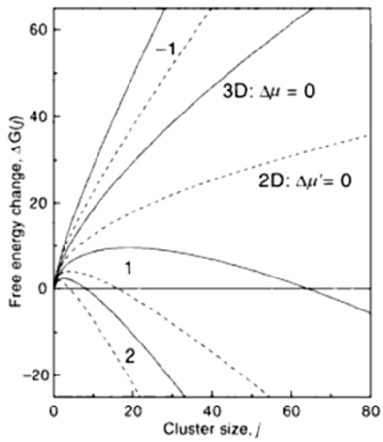

Figure 2.3: Free energy curves of nucleation ΔG (j) *for 3D (full line) and 2D (dashed lines) clusters and for different levels of supersaturation [34].*

These considerations are not completely realistic, since it is questionable, how macroscopic concepts like surface energies are appropriate for monolayers. At this point, an atomistic approach should be applied, which still is in agreement with macroscopic thermodynamics for large *j*. Here kinetics comes into play. The atomistic processes are described by rate equations, which have in the simplest case solutions in Arrhenius form:

$$q = q_0 \cdot \exp\left(-\frac{\Delta G^*}{kT}\right) \qquad (2.12)$$

where q could be the nucleation rate or a concentration along the surface, q_0 is a pre-exponential factor, which contains e.g. frequencies or mobilities. This equation shows the connection between thermodynamics and kinetics: The supersaturation as the driving force is contained in the exponential term. The rate model developed by Venables [36] adds non-linear terms for surface processes (Fig. 2.5), nucleation, and growth. These processes are governed by energies, which appear in the exponentials, and by frequencies and entropic pre-exponential factors. The equations can be plotted in so-called Arrhenius plots. These plots then reveal the dominant factors in certain temperature regimes.

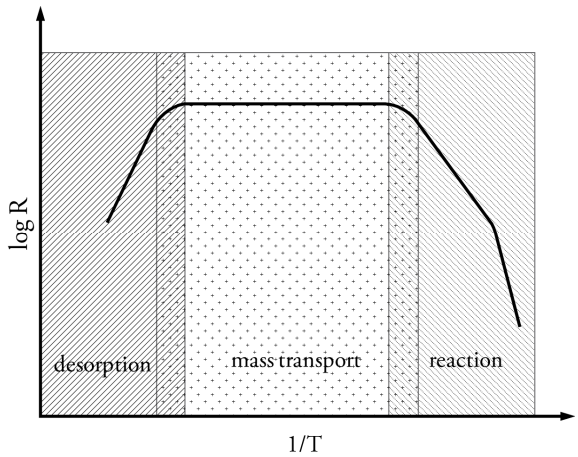

Figure 2.4: A schematic Arrhenius plot of the growth rate. *The slope is a measure of the activation energy. At low temperature the growth is reaction controlled, here with two different activation energies. At intermediate temperature mass transport governs the growth rate, and at high temperature desorption takes place and the growth rate drops. Drawn after [37].*

In Figure 2.4, a schematic Arrhenius plot of the growth rate is shown. At very high temperatures atoms tend to desorb, the growth rate drops. At intermediate temperatures the growth rate is governed by mass transport and stays constant with temperature. Ordinary epitaxial layer growth is performed in this temperature region. At lower temperatures surface reactions control the growth rate, which decreases with decreasing temperature. Nanowires are often grown in this temperature range, since here, layer growth is suppressed.

2.2.2 Epitaxy

The word epitaxy has its origin in the Greek words ”epi” (επι) meaning ”above” and ”taxis” (ταξισ) meaning “in an ordered manner”. It is a version of crystal growth where arriving atoms are incorporated at certain positions on the surface in relationship to the underlying crystal structure. Epitaxial growth is used to produce high quality single crystal layers with low defect density for electrical, magnetic or optical applications, which cannot be achieved otherwise [34]. Epitaxy of the same material as the underlying substrate is denoted as homoepitaxy, whereas growth of different materials on each other is called heteroepitaxy. For nanowires, the preferred growth direction is <111>B, meaning the terminating layer consists of group V atoms. To achieve nanowires vertically aligned to the substrate, substrates with {111}B orientation are used.

2.3 Surface Processes

When atoms arrive on a surface the following processes can occur (Fig. 2.5): Atoms can adsorb (a) and desorp (b) later on. Once they are adsorbed, they can diffuse (c), until they meet other atoms and form nuclei (d) or incorporate at energetically favorable places such as step sites (e) or kink sites (f). Which of these processes happen preferentially depends on the surface properties, i.e. the roughness and the surface energy, the interaction between the substrate and adsorbate atoms, the temperature and the supersaturation.

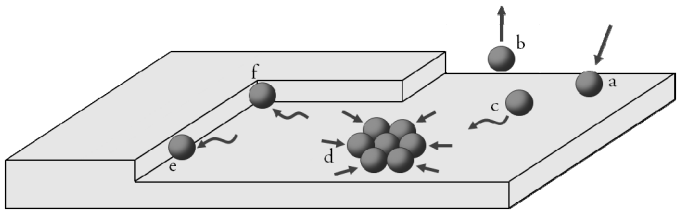

***Figure 2.5: Processes on the substrate surface**. a adsorption, b desorption, c diffusion, d nucleation, and incorporation e at an edge or f at a kink.*

2.3.1 Surface and interface energies

The energy at an interface between two phases is in general higher than in the volume, since bonds between atoms do not continue in the same way as they do in the bulk. If one of the phases is vacuum, the term surface energy is used, but it is commonly applied to any interface between solid and gas or liquid and gas, respectively. Any body tries to minimize its energy, therefore surface areas are minimized or, if that is not possible, surfaces with minimal surface energies are preferentially formed. Spherical droplets formed by liquids are an example for the first, facet formation of crystals for the latter, where planes with the least dangling bonds represent larger areas of the surface. The way two materials combine depends hence on their surface energies and their interface energy. The coverage of material *A* by the material *B*, is determined by the relation of the surface energies γ_A, γ_B and the interface energy γ_{AB}. If the formation of the interface and the surface *B* has a lower energy than the surface of *A, B* will cover *A* completely:

$$\gamma_A > \gamma_{AB} + \gamma_B \qquad (2.13)$$

This 2D growth is called Frank-Van der Merwe growth mode. If it is energetically more favorable to expose more surface of A, than forming the interface and surface of B ($\gamma_A < \gamma_{AB} + \gamma_B$), islands of B will grow, in the so-called Vollmer-Weber mode.

If the energies are in the same order of magnitude, strain plays a role as well. In the Stranski-Krastanov mode, a wetting layer is formed with islands on top, which compensate for strain.

2.3.2 Surface diffusion

Surface diffusion is an important factor in crystal growth, since it is responsible for parts of the material supply. How atoms move on a surface depends on the interaction of free atoms with the surface atoms, i.e. in macroscopic terms the surface energy, temperature, pressure, and availability of energetic sinks, such as steps and kinks. An important measure is the diffusion length Λ_s, which determines the distance atoms can cover before they are incorporated or desorbed [38]:

$$\Lambda_s = \sqrt{D_s \tau_s} \tag{2.14}$$

where D_s is the surface diffusion coefficient and τ_s is the mean time of residence of the adatoms, both terms depend via Arrhenius-equations on the activation energies for surface diffusion E_{sd} and desorption E_{des}, respectively. So Λ_s can be expressed as:

$$\Lambda_s = a \exp\left(\frac{E_{des} - E_{sd}}{2kT} \right) \tag{2.15}$$

with a being the mean distance between two adsorption sites. In nanowire growth, the diffusion length determines the collection area, i.e. the area from which atoms can contribute to growth, and thereby the growth rate.

2.4 Size Effects

In nanowires, atomic level is not yet reached. To give an idea: a 50 nm thick and 1 µm long InP nanowire, for example, contains about 70 million atoms. The seed particle contains 1-2 million atoms. A bilayer (layer of In and P atoms) in a nanowire contains about 7000 atoms. Some definitions call this range therefore "mesoscopic" [39], since it lies in between continuum and molecular effects. Still, the size has not only an effect on the electronic and optical properties (as mentioned in the Introduction), but also thermodynamically.

A crucial size effect is the increase of the surface-to-volume ratio with decreasing size. Thus, the surface properties get a larger influence on the overall properties of the particle. One important consequence is polytypism in nanowires. III/V materials – except nitrides – crystallize in bulk in ZB, WZ is not stable. In nanowires, however, depending on the growth conditions, WZ [40, 41] and even more polytypes such as 4H and 6H can be observed [30, 41-44]. This is due to WZ having lower surface

energies than ZB, which is in this size range of larger importance than the higher bulk energy [45-48]. Some reports show that the tendency to form WZ increases with decreasing NW diameter [46, 49-52].

The curvature of a particle has a crucial effect on the vapor pressure, the melting temperature and the phase diagram. On a convex surface (a large curvature, i.e. a small radius), the atoms are more prone to desorption, since they have less bonds to neighboring atoms. This leads to a dependency of the vapor pressure on the radius r of the particle, which is described by the Gibbs-Thomson-effect:

$$p(r) = p_{\infty} \exp\left(2\sigma\Omega / rkT\right) \qquad (2.16)$$

with p_{∞} being the vapor pressure above a flat surface, σ is the surface energy density and Ω the atomic volume.

The Gibbs-Thomson effect influences as well the growth rate of nanowires. As [53] and [54] describe, the Gibbs-Thomson effect causes a decrease in growth rate with NW diameter below a certain diameter, since the vapor pressure of growth species increases, so less atoms enter the particle and the supersaturation is reached more slowly.

For the same reason, the melting temperature is depressed with shrinking size [55] as well as the solubility [56] of elements in each other, in general, phase boundaries in phase diagrams are shifted to lower temperatures and lower solubilities [57]. Still, in most cases, the threshold diameter, below which these effects become significant are mostly a few nanometers. Furthermore, a surface starts to melt earlier than the bulk [58]. Considering nanoparticles having a high surface-to-volume ratio, they are more prone to premelting.

Anyway, one should be careful when one applies the terms of solid and liquid state in this size regime. The small crystal can be seen as short-range ordered areas, which use to appear in liquids as well. Brownian motion, diffusion and vapor pressure lead to a quick exchange of atoms between two phases. So it is hard to distinguish between the two states. Still, there are a number of examples, which show that there is a difference in properties whereas a particle is solid or liquid [59-61].

3 Fabrication Methods

In this chapter, the methods applied for nanowire fabrication are introduced. Nanowires in our studies were grown by metal-organic vapor phase epitaxy (MOVPE). This process is illustrated first, including growth system and precursors. We use seed particles to grow nanowires. These particles can be generated and deposited in several ways. Some of the most relevant are presented and explained here.

3.1 Metal-organic Vapor Phase Epitaxy

MOVPE[1] is the most common method for growth of epitaxial layers in industry due to its high throughput compared to molecular beam epitaxy (MBE) or chemical beam epitaxy (CBE). However, the control of the process is complicated and not yet fully understood (operators call it often a black box). The only detailed textbook on MOVPE is written by G. Stringfellow [62] and is the source of most descriptions here. The growth depends on parameters such as substrate temperature, chamber pressure, molar fractions of the precursors, and their cracking efficiency and total gas flow. Many of these parameters are interdependent in themselves. Nonetheless, during the last four decades much development has taken place and the control of the process is now on a high level. Still, every machine is unique and leads to slightly different growth. In the next two subsections, the growth system will be explained, and then the precursors are presented in detail.

[1] The name comes from the precursor molecules that are used in the process. These are metal-organic compounds, where the metal (the growth species) is surrounded by organic functional groups. These precursors are cracked in the growth reactor in a vapor phase. Other names are organometallic vapor-phase epitaxy (OMVPE) or metal-organic chemical vapor deposition (MOCVD). We prefer MOVPE to underline the epitaxial character of the growth.

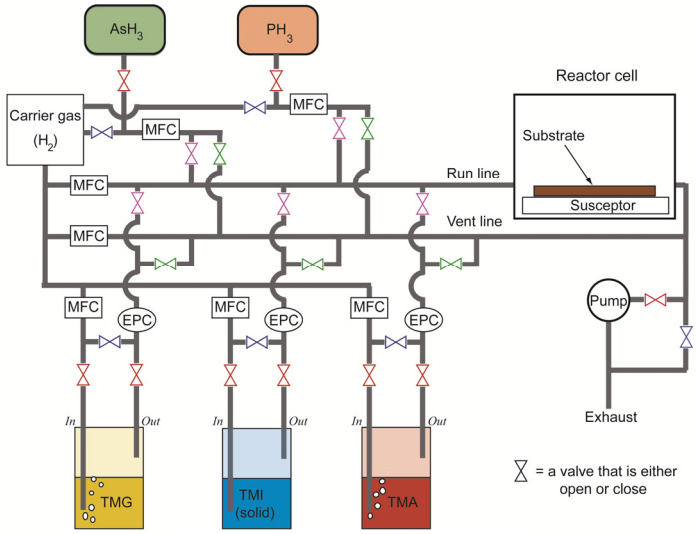

Figure 3.1: Schematic of a MOVPE system*. Color coding of the valves: red valves are open and blue are closed when the source is used, and vice versa when it is not in use. Pink valves are opened when the source shall be fed to the reactor and the green valves are closed at the same time. Otherwise the flow from the sources is led through the vent line to the exhaust [Courtesy of J. Bolinsson].*

3.1.1 The growth system

The essential components of the MOVPE growth system are the reactor, the carrier gas, the precursors, the heating and the plumbing system including the valve system as well as the pressure and flow control.

The "heart" of the MOVPE system is the reactor. Here, the substrates are positioned, the temperature is applied, the precursors are mixed and cracked, and eventually the growth takes place. The carrier gas (H_2 or N_2, in our case H_2) transporting the precursor gases flows over the heated sample holder (susceptor) to the exhaust. At the solid surfaces of the reactor (susceptor, sample, wall) the velocity of the gas is zero, since the flow is laminar [63]. As a consequence of this boundary condition, a stagnant boundary layer is built up above the susceptor, where the velocity of the flow is decreased and the mass transport happens only by gas phase diffusion [63]. There are several types of reactors, e.g. with horizontal or vertical flow direction; in this work a cold wall horizontal reactor was used. The susceptor consists of an inert, high temperature stable material such as graphite or refractory metals, and can be heated by radio frequency, resistivity heating, or infrared lamps. A schematic outline of a MOVPE system is given in Figure 3.1.

The system can be operated at atmospheric or at lower pressure down to a few tens of mbar. The total pressure influences the probability of parasitic reactions in the gas phase, the thermodynamics of the growth, and the diffusion of the growth species. The standard pressure of our systems is set to 100 mbar.

3.1.2 Precursors

The precursors are fed to the reactor in separate lines. Gas sources (often used for group V materials) are provided from gas bottles. Metal-organic (MO) sources are provided in so-called bubblers, which are kept at a certain temperature. A carrier gas is led through the liquid or solid source material, thereby saturated with molecules. The molar fraction fed to the reactor is then determined by the source flow, which is controlled by mass-flow controllers (MFCs). In addition, for MO sources, the molar fraction depends on the amount that is taken up by the carrier gas. It is determined by the vapor pressure of the precursor, which is controlled by the temperature, and the source pressure. The latter is controlled using electronic pressure controllers (EPC).

Two types of precursors are used in MOVPE. MO sources can be used for providing both group III and group V materials. Common group III sources are sources with short alkyl groups, such as Trimethyl-Gallium (TMG), Triethyl-Gallium (TEG), Trimethyl-Indium (TMI) or Trimethyl-Aluminum (TMA), amongst others. Typical MO-sources for group V materials are Tertiabutyl-Phosphine (TBP) and Tertiabutyl-Arsine (TBA). For group V materials, hydrides are often used instead, where the group V atom is surrounded by three hydrogen atoms, such as AsH_3 or PH_3.

The reason to use quite complicated molecules instead of direct evaporation of elemental sources is the controllability and handling. The evaporation of pure materials is difficult to govern, since they mostly have a high vapor pressure and low melting points; i.e. the cracking of molecules at a confined place is more convenient, even though the process is not yet completely understood.

The cracking, i.e. the dissociation of the precursors, occurs in multi-step reactions, until the metal or group V atom is set free [64]. This process can happen homogeneously, i.e. in the gas phase, or heterogeneously, i.e. on the substrate surface. The latter is the preferred situation, since homogeneous pyrolysis would cause parasitic reactions and the molecules would not end up in the growing crystals. The cracking efficiency of the precursors is a crucial factor in MOVPE and not only influenced by the temperature and surfaces, but also by the combination of precursors; so does for example the presence of TMI increase the cracking efficiency of PH_3 [65]. If the cracking efficiency is low at the desired growth temperatures a large excess of precursor has to be fed to the reactor to provide enough material for growth. If, however, it is so high at the desired growth temperatures that

homogeneous pyrolysis takes place, material will be consumed by parasitic reactions. Therefore, the applied growth temperatures have to be taken into account for the choice of precursors. An additional issue is the incorporation of carbon into the growing crystal, especially at low temperature growth. This has been attributed to the formation of CH_3 radicals, that decompose to carbon [66]. H radicals from the pyrolysis of group V hydrides or a higher total pressure help to avoid that process. The use of precursors with longer alkyl groups, such as TEG, reduces the effect as well.

3.2 Particle Fabrication and Deposition

Seed particles for nanowire growth can be produced in several ways. Purity, size selectivity, and position control are decisive factors for selection of a method. In the following, some common particle fabrication and deposition methods are introduced: particles formed from thin-films, lithographically defined particles, colloidal particles and aerosol particles [I]. Table 3.1 gives an overview of the different methods, their advantages, and drawbacks.

***Table 3.1: Overview** of the general characteristics of different particle types [I]*

Particle Type	Diameter range	Diameter Control	Density Control	Position Control	Throughput	Cleanliness	Simplicity	Cost
Aerosol Spark Generated (**SDA**)	Limited	Very Good	Very Good	Very Limited	Reasonable	Very Clean	Reasonable	High
Aerosol e/c Generated (**ECA**)	Broad	Very Good	Very Good	Very Limited	Reasonable	Very Clean	Reasonable	High
Colloid Directly Deposited (**DDC**)	Very Broad	Very Good	Limited	Uncontrolled	Very High	Contaminated	Simple	Low
Colloid Electrospray Deposited (**ESD**)	Very Broad	Very Good	Very Good	Very Limited	Low	Contaminated	Reasonable	High
EBL Generated (**EBD**)	Limited (small difficult)	Very Good	Very Good	Very Good	Very Low	Contaminated	Reasonable	Very High
Thin film Generated (**TFA**)	Broad	Very Limited	Very Limited	Uncontrolled	Very High	Very Clean	Simple	Medium

3.2.1 Particles generated by annealing of thin films

In this method, a thin metal film with a thickness in the range of a few Ångströms to a few nanometers is deposited by evaporation on the substrate. The layer forms islands of various sizes at elevated temperatures due to surface diffusion, coalescence and Ostwald-ripening [67]. This annealing step is mostly done *in situ* prior to growth. The size and surface density of the particles depends on layer thickness, annealing temperature and time, and the surface properties of the materials. Thus increased thickness [68], higher temperature and/or longer annealing time [8] lead to larger particles and lower surface density. Shorter annealing time and higher temperatures lead to narrower size distributions; with appropriate chemical treatment even almost monodisperse distributions can be achieved [69]. Still, the surface density and size distribution can only be controlled to some extent. This method is simple, clean and inexpensive and is mainly suitable for studies on the influence of the nanowire diameter, since it provides several particle sizes at the same time.

3.2.2 Lithographically defined particles

The definition of particles by lithography can be considered as an extension of the thin film method. It allows for precise control of size and position of the particles [70] by transfer of a pattern on the substrate before metal deposition. There exist numerous lithographic methods. The most common is surely photolithography. Similar to that is electron-beam lithography (EBL), but with a higher resolution and effort. Furthermore nanosphere lithography, where patterns of beams serve as mask, and nanoimprint lithography, amongst others. EBL is the method used here, and therefore the only one described. A resist is spun onto the substrate. The sample is then exposed to an electron beam. The electrons change the solubility of the photo resist, in this way the pattern is written into the resist. By development and subsequent dissolving of the resist, a pattern is left on the substrate, e.g. resulting in a surface pattern with holes. Then, a metal layer is deposited on the surface. After removing the photo resist completely, the so-called lift-off, metal disks remain on the surface where there had originally been holes in the photo resist. This is a time consuming and expensive method. In addition, remnants of the chemical processing may stay on the surface.

3.2.3 Colloidal particles

These particles are metal particles fabricated by a chemical reduction process [71] and stabilized in a colloidal suspension. Colloidal particles are commercially available in a wide range of sizes. Particles can for example be directly deposited onto the substrate or by electrospray-deposition. If the particles are directly deposited, a droplet of the solution is placed on the substrate for a certain sinking time, and then rinsed with DI water and blown dry. Often a surfactant layer of Poly-(L)-lysine (PLL) is needed to compensate for electrostatic repulsion [72]. The solutions can be spun on the substrate for a more homogeneous distribution. This method is simple, but suffers from contamination due to stabilizing ligands and PLL, and an inhomogeneous surface distribution. The reproducibility of the particle density is increased by deposition via electrospray [73]. In this method, the solution is sucked through a capillary and split up into droplets in an electric field. Ideally, one droplet contains a single particle. The droplets are transported and dried in an N_2 stream and optionally annealed. Finally, the particles are deposited onto the substrate via an applied potential that attracts them to the surface. This leads to a homogeneous and controlled distribution of the particles. Compared to direct deposition, the amount of organic remnants is reduced, but the setup is more complicated.

3.2.4 Aerosol particles

A very clean and controlled method to produce particles is the aerosol technique. Material is evaporated, either by heating [74] a piece of material in a furnace or by spark discharge [75], where a high voltage between two electrodes consisting of the particle material causes a spark and thereby locally high temperature (Fig. 3.2). The vapor is then transported in an inert gas to a cooler region, where the material condensates and agglomerated particles, consisting of a number of so-called primary particles, form. These particles are size selected with the help of a differential mobility analyzer (DMA). Then the particles are sintered to compact particles in a second furnace and again size selected according to the desired size. After that. the particles are deposited by applying an electric field to the substrate. The number of particles deposited can be measured by an electrometer. This method is very clean and both the size and the surface density can be controlled accurately. In our group, we mainly use aerosol particles for nanowire growth.

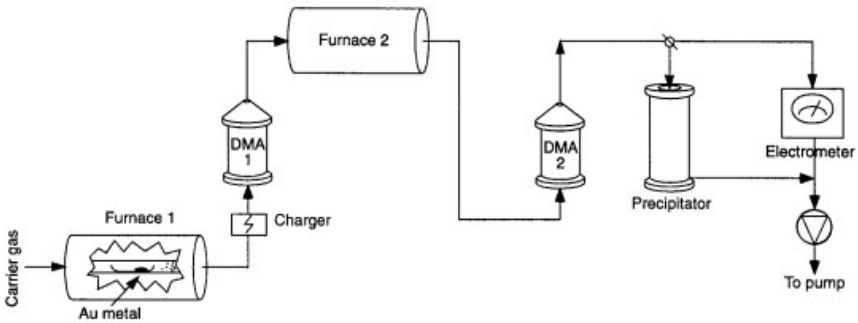

Figure 3.2: Schematic of the aerosol setup. *The evaporation of material happens in furnace 1 in the case of the evaporation/condensation method. In the spark discharge method, the furnace is replaced by a spark discharge chamber. After size selection of the agglomerated particles in DMA 1, they are sintered and reshaped in furnace 2, size selected for their final size in DMA 2, and the deposited in the electrostatic precipitator [from ref [74] with permission].*

4 Characterization by Electron Microscopy

Due to their small size, nanowires have to be characterized using special techniques with high resolution. In this work, electron microscopy is solely used for characterization. For topographical characterization scanning electron microscopy (SEM) is applied. Transmission electron microscopy (TEM) is used to investigate the structural and compositional state of the nanowires. SEM and TEM differ in the way they illuminate the sample and the geometry of signal detection: In SEM, a converged beam scans over a sample and signals are detected from the top. In TEM the sample is illuminated with a parallel beam and the transmitted signals are detected. First, the interactions of electrons with matter are introduced. Then, the general parts of the instrument are described for both SEM and TEM [2]. The different image modes of TEM are described more in detail, including conventional TEM (CTEM), high-resolution TEM (HR-TEM), scanning transmission electron microscopy (STEM) and analytical electron microscopy (AEM). Finally, *in situ* TEM is described, which enables nanowire growth while observing them.

4.1 Electrons for Characterization

From the concept of resolution for visible light according to the Rayleigh criterion, the resolution (meaning the smallest distance δ between to points that can be distinguished) is proportional to the wavelength λ:

$$\delta = \frac{0.61\lambda}{n \sin \beta} \approx 0.5\lambda \qquad (4.1)$$

with n being the refractive index of the medium and β being the semi-angle of collection of the magnifying lens.

[2] SEM is the workhorse in our laboratory, every sample is investigated using it. Nevertheless, nowadays the operation of SEMs is so intuitive that it does not need deep insight in the technique. Therefore TEM section got more room in this thesis.

This concept was the driving force to use electrons for imaging in the first place, since the energy E determines the wavelength of the electrons, as defined in de Broglie's equation [76]:

$$\lambda \approx \frac{1.22}{\sqrt{E}} \qquad (4.2)$$

That means high acceleration energies give short wavelengths and will result in higher resolutions compared to visible light (100 kV lead to an electron wavelength of about 4 pm). The dependence of the resolution on the wavelength is, however, not as simple as in Equation 4.1, since the Rayleigh criterion is not valid for electrons, due to its limitation to incoherent light (whereas electron sources produce coherent light). These extremely high resolutions from theoretical calculations have never been reached in electron microscopes, though. In fact, the limiting factor for resolution is not the wavelength, but the quality of the electron lens system and scattering of the electrons in the sample. Scattering is one of several effects, when electrons interact with a sample. The different interactions generate a whole bunch of signals, which can be used for different purposes. The primary electrons generate secondary electrons (SE), X-rays and Auger electrons via inelastic scattering; if they are scattered elastically, they are detected as backscatter electrons (BSE) (Fig. 4.1). Secondary and backscattered electrons are used for imaging in SEM. The transmitted direct beam and the elastically scattered electrons are used in TEM for bright field (BF) and dark field (DF) imaging, respectively. X-rays, Auger electrons and inelastically scattered electrons are used for analytical electron microscopy (see 4.5), i.e. chemical analysis, such as in energy dispersive X-ray spectroscopy (XEDS), since they are characteristic for elements and their bonds. Generated electron-hole pairs can be used for cathodoluminescence (CL). Not only useful signals are produced by the electrons, but also heat and beam damage in the sample are generated by inelastic scattering and "absorbed" electrons.

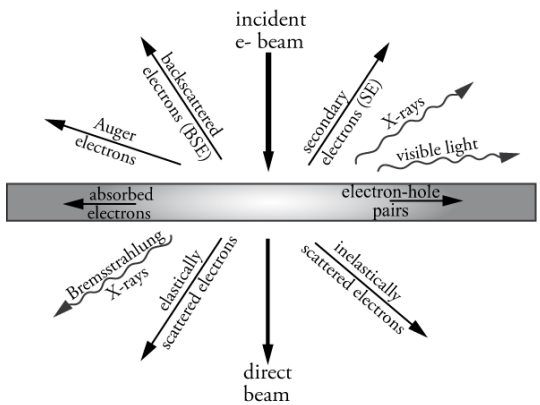

Figure 4.1: Schematics of the signals *created by radiating a specimen with high energy electrons. Straight arrows correspond to electrons, whereas wave arrows correspond to photons.*

4.2 The Instruments

The electron microscope consists mainly of four parts:

- The electron gun, which is used to generate and accelerate the electrons
- The lens system, which is used to focus the electrons onto the sample
- The sample, which the electrons interact with
- The detection system, which converts the signal of the electrons into a visible image

Since the sample and the detection geometry are different for SEM and TEM, they are treated separately in the corresponding sections 4.3 and 4.4, respectively.

The electron gun [77]: Electrons are set free via thermionic emission or field emission. In the first method, a wire (most often tungsten or LaB_6) is heated up so that the energy of the electrons exceeds the work function of the material and thereby the electrons can leave it. In the second method, electrons are extracted from a tungsten tip with the help of an electric field. Thermionic emitters are less expensive than field emitters, but the latter create a brighter electron beam with a narrower energy spread. The electrons are then accelerated by anodes to the desired energy. The instruments in this work are equipped with field emission guns.

The lens system [78]: Since electrons do not interact with any material in the same way as visible light does with glass, electron lenses are based on a different concept. Electron lenses are magnetic lenses that consist of a soft magnetic core with a hole in it, the so-called polepiece, surrounded by a copper coil. Current through the copper coil induces a magnetic field in the hole. The current controls the strength of the magnetic field and thereby the path the electrons take through the lens. The electrons move with a helical trajectory through the field due to the Lorentz force, with the result that magnetic lenses act like convex glass lenses. The quality of magnetic lenses is actually fairly poor compared to lenses for visible light; Williams and Carter [78] compare them with "using the bottom of a […] bottle as a magnifying glass". There are several lens defects, whereof spherical aberration, chromatic aberration, and astigmatism are the most important ones.

The first, spherical aberration, is the main error limiting the resolution. Spherical aberration is the effect that electrons, which are off-axis, are bent back towards the axis leading to image disks instead of image points and thereby limiting the resolution. By inserting apertures, the off-axis electrons are screened from the beam and image distortions are reduced. During recent years, a correction for the spherical aberration in TEM was developed, which leads to much higher resolution, but not all microscopes are equipped with one yet.

Chromatic aberration is caused by electrons with a spread in energy. The spread from the sources is very small and can be neglected. But inserting the sample into the electron beam produces electrons of a wide range of energies which are then bend differently by the following lens leading to a disk image (this holds for TEM, not for SEM).

Astigmatism is a lens error due to imperfect lenses. If the electrons sense a non-uniform magnetic field, the focal planes will be different for perpendicular rays. In practice, defocusing leads to distortions in different directions. Astigmatism can be compensated by stigmators, small magnets in the lens, which balance the inhomogeneities of the lens leading to a uniform magnetic field.

4.3 Scanning Electron Microscopy

In scanning electron microscopy, the sample is illuminated by the electron beam which scans over the surface due to deflection by scanning coils. The electrons of the beam interact with the sample. The sample has to be conductive, otherwise the electrons accumulate, which leads to charging effects, i.e. incoming electrons are deflected. For imaging, secondary electrons which come from areas close to the surface and backscattered electrons coming also from deeper regions are used. Secondary electrons give mainly information on the topography, since they only escape from regions close to the surface due to their low energy. Edges appear brighter due to the fact that more electrons are generated here. Backscattered electrons, however, also provide information on the composition, since heavier elements scatter electrons more than lighter elements. In the studies of this work, only the topography was investigated by SEM, so only imaging with secondary electrons (SE) was conducted. The emitted electrons are attracted by an electric field to a detector placed above or on the side of the sample. The signal is amplified and leads to an image. The acceleration voltage governs the probe size and the penetration depth, which both influence the resolution. A higher acceleration voltage leads in principal to a higher resolution, but also to a larger penetration depth (i.e. excitation volume). For SE, that means a smaller signal to noise ratio. To resolve surface features, it can therefore be more advantageous to use lower acceleration voltages. SEMs are mostly operated at 1-20 kV. The resolution of SEMs can be a few nm, depending on sample and conditions.

4.4 Transmission Electron Microscopy

In transmission electron microscopy the sample is placed in the middle of the ray path, i.e. between the two pole pieces of the objective lens (Fig. 4.2). The electrons interact with the sample and those transmitted through the sample are magnified and focused by the image lens system onto a fluorescent screen or to an appropriate detector, such as a CCD (charge-coupled device) camera depending on operation mode and purpose.

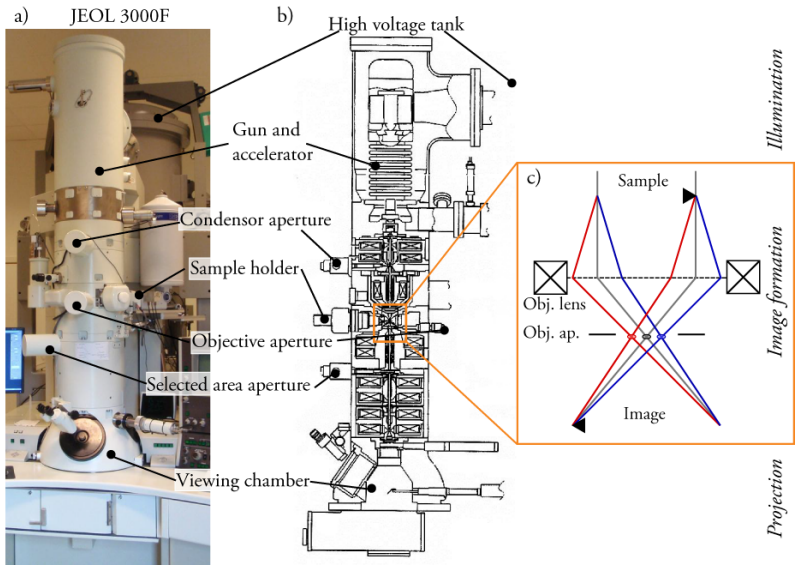

Figure 4.2: The JEOL 3000F TEM*. a) photograph of the instrument [Courtesy of G. Karlsson], b) schematic of the instrument c) ray diagram of the image formation [Courtesy of M. Ek].*

Since the electrons have to pass through the sample, it has to be sufficiently thin, i.e. thinner than about 100 nm depending on the material and the acceleration voltage. The interaction of the electrons with the material gives not only a projection image of the sample, but also information about the crystal structure via diffraction images, the composition via X-rays or energy-loss and can reveal the atomic structure in high resolution mode. The beam can even be converged and then scanned over parts of the sample, in the so called STEM mode, see 4.5. Fig. 4.2 shows the instrument with legends to the different parts. After the electrons are accelerated they pass the condensor lens and aperture and undergo the first crossover of the optical axis. By changing the strength of the condensor lens, the spot size and the illumination brightness is changed. The electrons then pass the objective lens, where they interact with the sample. The objective aperture is placed in the back focal plane and the first

image appears in the image plane of the objective, where the selected area aperture is situated as well. Finally they pass intermediate and projector lenses, where the image is magnified, before they hit the screen or the detector.

4.4.1 Image modes in conventional TEM

In conventional TEM, the aim is to apply a parallel beam, since then it is most coherent. In TEM imaging can be conducted in real space and in reciprocal space. Images in real space are bright field (BF) or dark field (DF) images, whose contrast formation is discussed in 4.4.2. The terms simply describe the shade of the vacuum in the image, bright and dark, respectively. Images in reciprocal space are formed by electron diffraction [79] at the lattice planes (it can also be seen as the Fourier transformation of the real image). So called Bragg diffraction scattering at a set of crystal planes gives maxima only at certain angles related to the crystal orientation. These maxima appear as spots; if the sample is tilted such that a zone axis[3] is oriented parallel to the beam, a regular pattern appears. This diffraction pattern gives information about crystallinity, crystal structure and lattice plane spacing. The diffraction pattern appears in the back focal plane of the objective lens, close to the objective aperture (see Fig. 4.2 c)). The spots are displayed on the screen, if the image plane is moved to the plane of the objective aperture by changing the focus of the intermediate lens, and the selective area aperture is inserted to choose the contributing part of the image. In practice, this happens automatically at the microscope when switching to diffraction mode.

4.4.2 Contrast formation in TEM

Contrast is the difference in intensity between two areas, which is determined by the amount of electrons per area reaching the viewing screen or the detector. Contrast appears, since the incident beam is scattered by the specimen [81]. In BF images, unscattered electrons contribute to the image (i.e. give bright areas). In DF, only scattered electrons, normally only those scattered at certain crystal planes, contribute to the image.

Two types of contrast can be observed in TEM: amplitude contrast and phase contrast. Both types may contribute to the image, but in most cases one dominates over the other. In conventional TEM and STEM amplitude contrast is the main mechanism and will be discussed first, phase contrast is used in HR-TEM.

---

[3] Zone axis: a crystal direction, which several families of crystal planes share [80].

Two mechanisms lead to amplitude contrast, mass-thickness contrast, and diffraction contrast. In mass-thickness contrast, contrast arises since electrons are incoherently scattered off-axis more at atoms with higher mass Z and more scatter events take place in thicker areas. That means for BF, areas of heavier elements or thicker areas appear darker. The opposite happens in DF. To enhance the contrast, an objective aperture might be inserted to exclude scattered electrons (and also aberrations due to off-axis electrons). Diffraction contrast gives information on crystal orientations, since it arises due to diffraction at crystal planes. The parts of the sample lying in diffracting crystal orientations appear dark in BF and bright in DF.

4.4.3 High-resolution TEM

High-resolution imaging can reveal the atomic structure of crystalline specimen by visualizing atomic columns, if a zone axis of the samples is oriented along the beam. HR-TEM makes use of phase contrast [82], which is present, if more than one beam contributes to an image. When the electrons interact with the sample they change their phase, so that an interference of several beams leads to phase contrast. The phase contrast can reveal the atomic structure, but is very sensitive to thickness, orientation and settings of the microscope. Since the microscope is not perfect, each point in the specimen is transferred into an extended region in the image. Those in turn overlap, so that every point in the final image contains information from many points in the image. This convolution can be described mathematically. The aim is to obtain a function, which can be used to determine the resolution, i.e. where the phase contrast image is still directly interpretable, taking the limitations of the specific microscope into account: the contrast transfer function (CTF). For convenience, those functions are transformed to reciprocal space (i.e. Fourier transformed) here, in dependence on the reciprocal lattice vector **u** (corresponds to 1/distance):

$$G(\mathbf{u}) = H(\mathbf{u})F(\mathbf{u}) \qquad (4.3)$$

$F(\mathbf{u})$and $G(\mathbf{u})$ correspond to the functions of the specimen and the corresponding area in the image, respectively. In real space, they are related by a point-spread function, which corresponds now to $H(\mathbf{u})$, the contrast transfer function. $H(\mathbf{u})$ describes how information in reciprocal space is transferred to the image. The CTF contains contributions from the limiting aperture, the attenuation of the wave and the aberration of the lens. The contribution of the lens aberration is here of main interest, dependent on the term $\chi(\mathbf{u})$, which contains the spherical aberration C_S, the overfocus Δf and the wavelength λ of the electrons, i.e. the influence of the acceleration voltage:

$$\chi(\mathbf{u}) = \pi\Delta f\lambda u^2 + \frac{1}{2}\pi C_S\lambda^3 u^4 \qquad (4.4)$$

Fig. 4.3 shows the contrast transfer function of the JEOL 3000F used in this work.

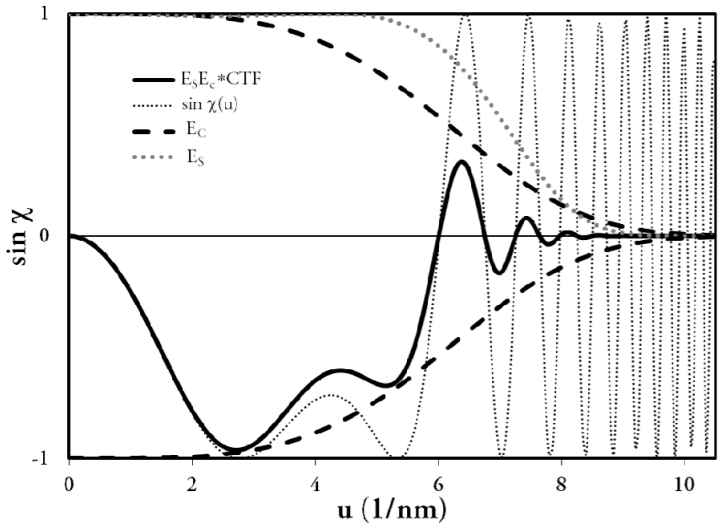

Figure 4.3: The contrast transfer function *for the JEOL 3000F with Δf_{sch} of -34 nm. E_S and E_C are envelope functions related to illumination convergence and defocus spread, respectively.*

For values smaller than $\mathbf{u}_1$, where the CTF equals zero for the first time, phase contrast images are directly interpretable. For higher values, special software is needed. So u_1 defines the resolution at certain C_S, λ and Δf. An optimum focus value, which balances C_S, is the Scherzer defocus:

$$\Delta f_{sch} = -1.2(C_S \lambda)^{1/2} \qquad (4.5)$$

At this value, all beams have a nearly constant phase at the crossover. The resulting resolution is the Scherzer resolution:

$$0.66\, C_S^{1/4} \lambda^{3/4} \qquad (4.6)$$

The Scherzer resolution of the microscope used in this work is 0.17 nm.

4.5 Scanning-Transmission Electron Microscopy

Besides parallel illumination, the beam can also be converged to a small probe by changing the lens currents [83]. This probe is then scanned over the sample (as in SEM) ("normal" imaging is not possible anymore, since the parallelism is destroyed). STEM images do not suffer from aberration and the contrast is better than in TEM. STEM is, however a time consuming technique and is therefore only used for special purposes, such as analytical electron microscopy (AEM) to achieve spatially resolved compositional information of the sample. The damage introduced to the sample might be higher than in CTEM, since the beam energy is highly concentrated, but the exposure time at one point is much less at the same time, which can even reduce damage by e.g. heating.

STEM mode offers BF, DF and high-resolution (different from the term high-resolution in 4.4.3, i.e. not phase-contrast mechanism) as well, there are some differences to CTEM, though. STEM BF images are noisier than TEM BF images, but it is easier to adjust brightness and contrast. In STEM DF, strongly scattered electrons contribute to the image, detected by a high-angular annular dark field (HAADF) detector. Using incoherent high-angle scattered electrons for imaging gives rise to a strong Z contrast from single atoms. Compared to TEM DF, where only a small fraction of the electrons are used for imaging, a higher amount of electrons is collected, which gives less noise.

4.6 Analytical Electron Microscopy

As introduced in 4.1 various signals are emitted during the interaction of electrons with the sample. In analytical electron microscopy, those signals which give information about the composition of the sample are used, such as the energy loss of the electrons in electron energy loss spectroscopy (EELS) or the X-rays in XEDS. The latter was used extensively in this work and will therefore be described in the next section.

4.6.1 X-ray energy dispersive spectroscopy

This method uses the fact that incoming electrons eject core electrons from atoms, electrons from higher energy levels fall down to the empty states. During the process X-rays with characteristic energies specific for each level in each element are emitted (Fig. 4.4).

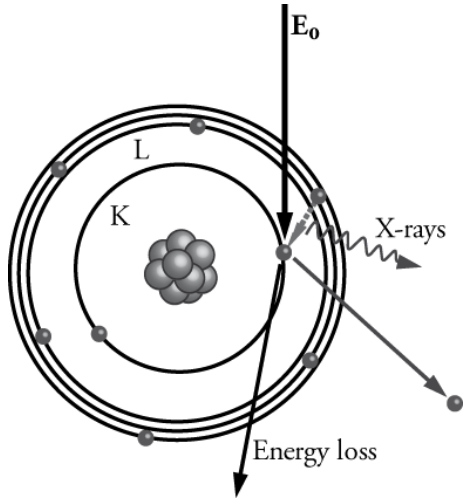

Figure 4.4: Generation of X-rays*. The beam electrons emit an electron from a lower level, an electron from a higher level falls down. This process emits X-rays with wavelengths corresponding to the energy difference between the two levels, which is characteristic for each element. The beam electrons lose energy during that process, which is used in EELS.*

The X-rays can thus be detected according to their energy and can then be correlated to the elements in the sample [84]; Figure 4.5 shows an example of an XEDS spectrum with designated elements. XEDS provides not only qualitative information on the composition of the sample, but also quantitative information. The concentrations C_i are extracted from the intensities I_i in the spectrum setting the intensities of a pair of elements in relation via the Cliff-Lorimer equation:

$$\frac{C_A}{C_B} = k_{AB} \frac{I_A}{I_B} \qquad (4.10)$$

k_{AB} is called the Cliff-Lorimer factor and is related to the atomic number, but also dependent on the system and the acceleration voltage. The absolute fraction of the components is obtained by:

$$\sum_i C_i = 100\% \qquad (4.11)$$

The k factors of two pairs are related by:

$$k_{AB} = \frac{k_{AC}}{k_{BC}} \qquad (4.12)$$

The k factors can be determined experimentally using standards or by calculations from first principles.

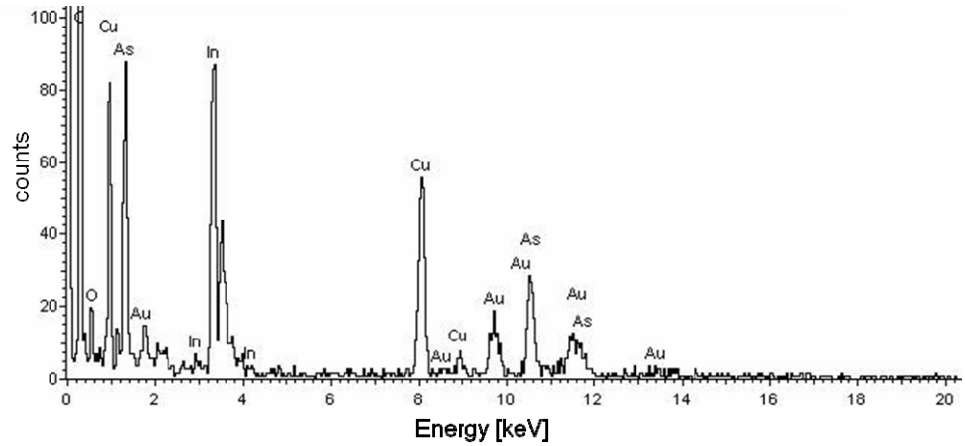

Figure 4.5: XEDS spectrum *(section) of an InAs NW seeded with Cu-particles on a Au-grid.*

To extract the intensities the background needs to be subtracted which may be done by geometrical estimation or background modeling. Nowadays the above calculations and values are automated in the applied software package. This makes the quantitative analysis very simple but bears the danger of trusting values without understanding and considering possible errors. The quantitative resolution of the equipment used lies within 2 at%. In combination with STEM mode, the composition can be mapped spatially resolved. The spatial resolution depends on the beam diameter and the beam spreading, which depends on the thickness of the sample and inversely on the beam energy.

4.7 *In situ* Transmission Electron Microscopy

During research visits at the IBM Thomas Watson Research Center in Yorktown Heights a special UHV-TEM was used, which enables *in situ* observation of nanowire growth. The microscope is a conventional Hitachi H-9000 operated at 300 kV and a base pressure of ~$2x10^{-10}$ Torr, which was modified by the group. Precursors are fed through capillary tubes into the polepiece, where the sample is mounted in a heating holder, as shown in Figure 4.6.

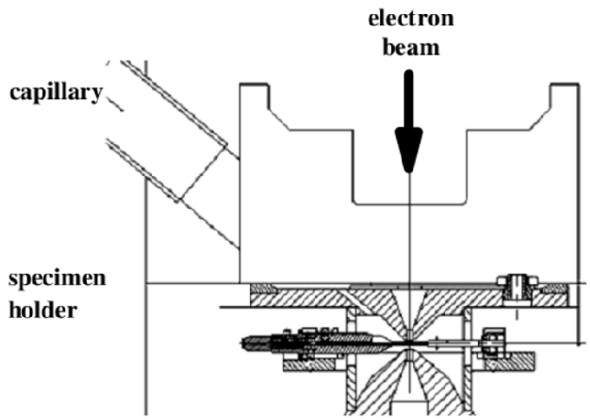

Figure 4.6: Schematic cut through the polepiece of the in situ UHV-TEM *with the heating holder inserted fFrom ref. [85] with permissio]n*

The pressure inside the microscope can be increased up to $5x10^{-5}$ Torr while observation is still possible. The amount of fed precursors is on the one hand controlled by the gauge, measuring total pressure, and by a mass spectrometer connected to the chamber. The temperature is controlled by the power fed through the sample, which has to be calibrated by a pyrometer before and/or after the growth. The samples are Si (111) bars, cut in desired zone axis, most often [1-10], mounted such that they are perpendicular to the beam and thus the particle/nanowire interface is perpendicular to the beam as well. DF imaging gives information about strain, phase changes, twins appear more clearly, and the oscillating corner (see 5.1) is visible more clearly. The images are recorded on video tape with a rate of 30 frames per second.

5 Nanowire Growth

As described in the introduction, research on semiconductor nanowires started about two decades ago, when Hiruma *et al.* reported on growth of GaAs nanowhiskers in their MOVPE [15]. Since then nanowire growth of group IV materials [18-20], of virtually all III/V materials [21, 22] has been demonstrated, as well as growth of II/VI nanowires [23, 24]. Since mainly III/V materials are grown by our research group, the focus of this chapter will lie on these.

The growth of nanowires has advanced of course, and heterostructures, both axial [86-90] and radial [91-96] have been realized (ref. [97] gives an elaborate overview). The fact, that nanowires of materials, which grow in bulk only in zinc blende (ZB) crystal structure, can also grow in wurtzite (WZ) structure has opened up a new field of research [98]: the control of crystal structure. Nowadays challenges for growers are doping [99-103], the tuning of the crystal structure [30-32, 40, 98], realization of new materials such as antimonides in nanowires [42, 104-108], and alternative seed particle materials [19, 20, 106, 109-118]. Even though nanowires have been grown with a high degree of control, many details of the growth mechanisms are not yet fully understood.

To generate nanowires, growth in one dimension has to be enhanced, while growth in the other dimensions needs to be suppressed. A number of mechanisms to explain semiconducting nanowire growth have been proposed during the last years. The most common is still particle assisted growth [21], furthermore selective-area growth [119] and oxide-assisted growth [120] are proposed. Mandl *et al.* evaluate these hypotheses thoroughly [110]. Since we apply particle assisted growth, only this mechanism will be discussed here.

5.1 Particle Assisted Nanowire Growth

Particle assisted growth is the prevalent method for semiconductor nanowire growth [21]. The particles can either consist of a metal other than the growth species, gold is here the most common material, or they consist of the group III metal, which is also incorporated into the nanowire, in the so-called self-seeded growth. Experimentally, metal particles are deposited onto a substrate (Fig. 5.1a)) (for particle fabrication and deposition methods see 3.2). After this, the substrate is transferred to the growth chamber.

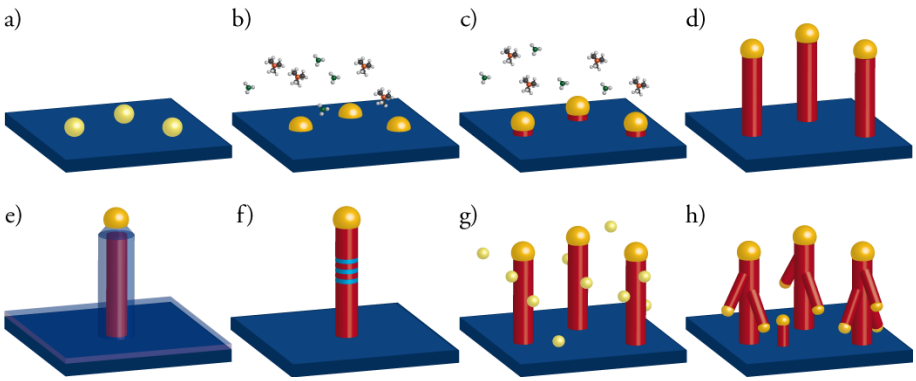

Figure 5.1: Schematic of the particle assisted nanowire growth process*. a)-d) and possible advanced structures e)-h). a) Particles are deposited on the surface, b) the source molecules are fed to the reactor and the particles form an alloy until they are supersaturated and c) solid nanowires are precipitated at the interface between substrate and particle, d) NWs grow as long as precursors are supplied. e) and f) by changing growth temperature and material e) radial and f) axial hetero-structures can be grown. Branched nanowires can be fabricated by g) deposition of a second generation of particles and then h) a repetition of the growth process.*

For self-seeded growth, the particles are often formed *in situ* by accumulation of group III to droplets. Then the source material is fed to the sample at elevated temperatures (Fig. 5.1 b)). The growth process is understood as follows: The particles serve as preferential deposition sites and form an alloy with the growth species (mostly group III). As soon as the particles are supersaturated, the excess material precipitates at the interface between particle and substrate (5.1 c)). The 1D crystals grow as long as source material is provided (5.1 d)). The preferential growth direction of III/V nanowires is the <111>B direction [4]. Under certain conditions they can be forced to grow in other directions [121]. Using {111}B substrates leads to vertically aligned nanowires.

Heterostructures, meaning a combination of different materials can be produced by changing the source materials and in case also the growth temperature. Increasing the temperatures to layer growth conditions, enhancing vapor-solid growth on the sidewalls leads to radial heterostructures (5.1e)). Such core-shell structures have been realized for many materials combinations, such as Si/Ge [92], GaAs/$Al_xGa_{1-x}As$ [94, 122, 123], Si/GaP [91], GaAs/$Ga_xIn_{1-x}P$ [93], InAs/InP [95, 96].

[4] B denotes the termination with group V atoms, whereas A denotes termination with group III atoms (see even 2.2.2)

Axial heterostructures can be produced as well for many material combinations (5.1 f)). Here, atomically sharp interfaces could be reached in InAs/InP [86, 124], GaAs/GaP [125, 126], and Si/Ge [88]. In other combinations a sharp interface is difficult – if not impossible – and a graded interface occurs, which can be explained by a reservoir effect of the particle [127]. This is normally a severe problem in Si/Ge heterostructures [128, 129], and in III/V materials, where group III is switched, which have a high solubility in the particle, such as InAs to GaAs [127, 130] or InAs to GaSb [90]. Recently, however, Dick *et al.* showed in InAs to GaAs heterostructures, that the reservoir effect can be overcome by carefully emptying the particle of the previous material before switching to the next [131].

Furthermore, kinking at the interface is an issue [89], due to combinations of surface energies which lead to the formation of a compact nucleus. This problem has partly been overcome e.g. in InAs on GaAs by crystal structure tuning [132] or by the insertion of an interlayer [IV],[133] (see 5.5.1).

A great advantage of nanowires is that combinations of highly lattice mismatched [5] materials can be realized, which would not form in bulk or thin films due to high strain. In nanowires, however, this strain can relax due to their small footprint [134]. GaAs/InSb heterostructures with lattice mismatches as high as 14.6% have been realized without formation of dislocations [105]. Also group IV and group III/V materials are possible to combine. In thin films, their combination is difficult, since anti-phase boundaries in the polar III/V material might form due to single atomic steps in the non-polar group IV material [135, 136]. This problem does not exist in nanowires due to their small cross section. Several "hybrid" nanowire heterostructures have been realized [89], as described in detail in 5.5.1. Heterostructure nanowires open up new material combinations and thereby new applications. Tunnel devices can be realized [90] due to sharp interfaces between materials with different band gaps, as well as single electron transistors [137].

The state of the seed particle has been under discussion for some time. The mechanism proposed by Wagner and Ellis [9], vapor-liquid-solid (VLS), assumes a liquid particle. Following this assumption, nanowires have been grown above the eutectic temperature [6]. It was found, however, that nanowires even grow below the eutectic temperature [138-140]. This goes along with a drop in growth velocity, indicating a solid particle, since the diffusion through a solid particle is slower than through a liquid particle [59]. In *in situ* TEM investigations, it was found that both

---

[5] lattice mismatch is the difference in lattice constants a_A, a_B of two materials *A* and *B* forming a heterostructure and defined by $(a_B - a_A)/a_B$

[6] The eutectic temperature is the lowest temperature, where an alloy exists as liquid

solid and liquid particles can exist at the same sub-eutectic temperature [60, 61]. In the meantime, the state of the particle is not considered to be that important anymore, especially since it is questionable how much on can distinguish between solid and liquid at the nanoscale (see 2.5). Therefore, the more general concept of preferential interface nucleation (PIN) was proposed [141]. The concept considers the state of the particle as not important, but its stability and the ability to collect material are. Furthermore, the nucleation occurs at the triple-phase boundary (TPB) (where vapor, particle and nanowire meet), since the Gibbs free energy of nucleation can be smallest there and the local supersaturation is relatively high. Those factors together lead to unidirectional growth. After nucleation, the addition of a material is quick compared to the nucleation and occurs as step-flow [142, 143]. Step-flow means, that the growth front of the new layer (usually a bilayer) moves along the plane from one side of the nanowire to the other.

Quite recently, however, it has been shown by *in situ* TEM independently by three scientific groups [27, 144, 145], that nanowire growth is more complicated: The morphology of the growth interface changes periodically. Small facets are formed at the edges of the nanowire (Fig. 5.2 a), c), d)). They shrink (material precipitates), then nucleation and growth of a (bi-) layer occurs quickly at the growth front. Material is dissolved and the facets return to their maximum size and start to shrink again (Fig. 5.2 b)). This phenomenon has been observed in the self-seeded growth of Al_2O_3 nanowires [144], Au-seeded growth of Ge nanowires [27, 145]; for Si nanowires seeded by several Au alloys, and even Au-seeded GaP nanowires [27]. These three scientific groups have different explanations and models for their observations. Oh *et al.* [144] suspect that the rim is dissolved to provide oxygen for the growth of a layer on the nanowire. They assume that nucleation still takes place at the TPB. Gamalski *et al.* [145] and Wen *et al.* [27] dedicate the formation of the truncations to thermodynamic effects. The size of the truncated facet is a measure for the supersaturation in the particle. Both state that the nucleation of the layer takes place away from the TPB. The main difference between these two models is, that the first assume that the small facet is atomically rough, and can therefore change shape easily, whereas the second suppose that the small facet can easily equilibrate due to lower nucleation barrier at the TPB. These findings radically change the view on nanowire growth mechanisms and make new models for stacking fault formation and polytypism necessary.

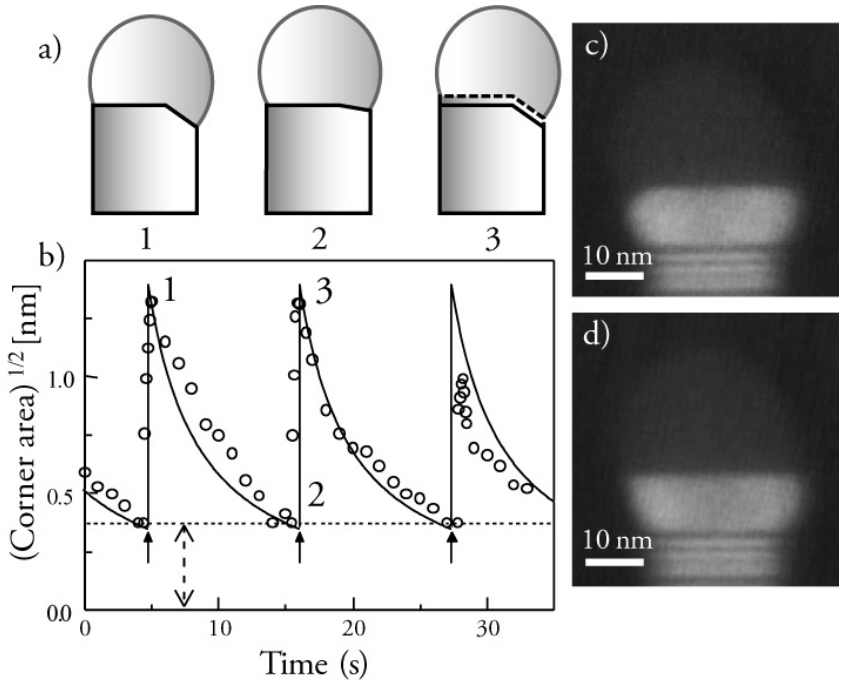

Figure 5.2: Peridically changing growth interface. *a) Schematics of the cycle of facet formation and growth. In stage 1 the facets are a their maximum dimension. They decrease (i.e. atoms deposit on the facets), until the growth front is almost flat (stage 2). A monolayer (bilayer) nucleates and forms and the facets switch back to their maximum dimension (stage 3). This step is very quick compared to the time between stage 1 and 2.b) The change of corner area with time. The numbers correspond to the stages in a). The arrows mark the formation of a bilayer. [modified from ref [27] with permission.] c) and d) DF images of a growing GaP NW: c) facet at maximum size, d) facet size minimized.*

5.2 Gold Seeded Nanowire Growth

Nanowires have been grown from gold particles for years. Up till now, no alternative material has been found which is as versatile. Au leads with almost all (semiconducting) materials to epitaxial nanowire growth, mostly in a wide parameter window [21]. The reason for the high versatility has not been fully understood yet. It is not clear, which property is the decisive one for successful nanowire growth or whether it is rather the unique combination of properties that gold possesses [146]. These properties are chemical inertness, thermal stability, the ability to form liquid alloys with a large number of growth species, softness, which enables good particle/wire alignment even in VSS growth mode.

Different scientific groups use various methods to prepare gold seed particles for nanowire growth. We wondered how comparable the results of different groups are, if different preparation methods are used. Therefore we studied the influence of different gold particle preparation methods on growth of GaAs nanowires [I] and on their optical properties [26].

5.2.1 Influence of particle preparation methods on growth of GaAs nanowires

Six different particle deposition methods were tested, namely aerosol particles generated by evaporation/condensation (ECA) and by spark discharge (SDA), colloidal particles, directly deposited (DDC) and electrosprayed (ESC), particles defined by electron beam lithography (EBD) and annealed thin films (TFA) (for preparation methods see 3.2).

Interestingly, we found, that the particle type has little influence on the nanowire growth when it comes to growth rate (Fig. 5.3) and crystal structure. Differences occur only in incubation time and in sensitivity to annealing. The incubation times are shortest for SDA particles, followed by ECA and ESD. DDC and EBD take the longest time to incubate (Fig. 5.4). This result suggests that the cleanliness of the particles influences the nucleation. Aerosol particles are by far the cleanest particles. For the other types, the amount of remnants seems to be so high, that they are not removed during annealing. So they influence the surface and the gold/substrate and gold/precursor interaction and thereby slow down the incubation. The difference in incubation time dependent on the deposition method of colloidal particles show, that remnants are well reduced during electrospraying; whereas direct deposition is by far dirtier as PLL is used in addition, which is known to change the surface properties notably [121].

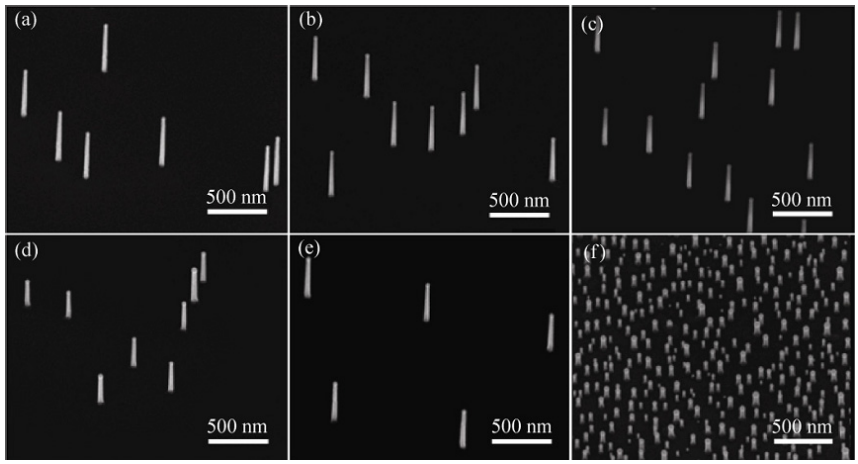

***Figure 5.3: Growth from different particle types**. SEM micrographs of GaAs nanowires grown at 430 °C for 4 min from different seed particles with diameters of 30nm: a) Spark generated aerosols b) evaporation/condensation aerosols c) directly deposited colloids d) electrosprayed colloids e) EBL patterned, and f) particles from annealed thin film [I]. The difference of the nanowires in f) compared to the others is due to the higher surface density. Sample tilt 30°.*

Furthermore, the state of the particles in terms of crystal structure is different before they are inserted into the growth reactor. Aerosols contain less grain boundaries than colloids. EBD and TFA particles could not be investigated by HR-TEM, since they form *in situ*. One may assume that even their crystal perfection differs from the other particle types. The amount of defects determines the diffusion in the particle, which is responsible for the mixing of Au and Ga. So even after the pre-growth annealing step the particles may not have all the same state, composition and surface, leading to a variation in incubation time. After 4 min growth time, however, the differences in length due to incubation time are diminished.

The largest difference between the particle types can be observed in the behavior during annealing. At 80 nm size for all particle types, splitting of particles into small ones can be observed. The patterns of EBD are often irregular for this diameter. This means that particles have moved around, which is certainly true for the other particles types as well, but cannot be observed, since they are positioned randomly. Nanowire growth from aerosol and colloidal particles is not remarkably affected, whether an annealing step is included or not. The NWs grow straight and vertically-aligned at all temperatures. They are only slightly shorter without pre-growth annealing step, since processes such as evaporation of impurities and alloy formation happen at growth temperature and during "growth time" and at lower temperatures.

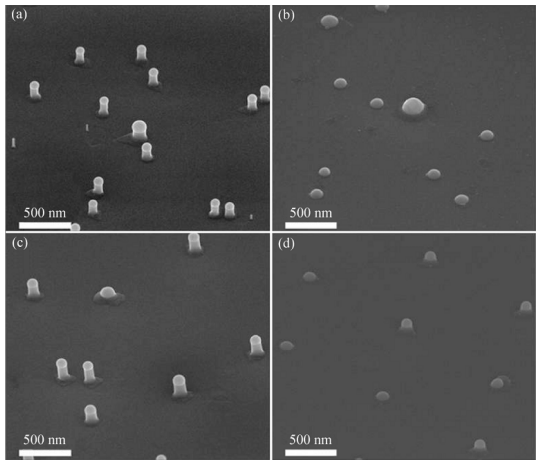

***Figure 5.4: Differences in incubation times**. SEM micrographs for samples after 1 min of growth at 430 °C for 80 nm sized (a) ECA, (b) DDC,(c) ESC, and (d) EBD particles [I]. Sample tilt 52°*

EBD and TFA particles, however, are strongly affected by the annealing. Without an annealing step many nanowires grown from TFA particles are "crawling" or kinked at all growth temperatures. NWs from EBD particles grow only at 480 °C successfully; otherwise they are kinked, or have a delayed nucleation. At 480 growth temperature, the pattern of the 80 nm sized NWs is even conserved and the samples are of better quality compared to those which include an annealing step of 650 °C. These effects are not surprising, since EBD and TFA particles form during the annealing step. The highest growth temperature, however, seems to be high enough to "anneal" the samples and at the same time low enough to avoid movement.

5.2.2 Influence of particle preparation methods on the optical properties of GaAs nanowires

In addition to general growth effects of the particle type, we investigated the influence on the optical properties by cathodoluminescence spectroscopy (CL) [26]. In order to improve the emission intensity and stability in the electrical beam, a thin AlGaAs shell was added after the growth of GaAs [147]. In this case, only 30 nm sized particles were used; TFA particles were excluded, since the variation in diameter makes the results less comparable. In addition to ECA, SDA, EBD, DDC and ESC, electrosprayed particles, which were annealed after atomization and before deposition (ESAC) were used to investigate possible improvements of the cleanliness due to this annealing. In particular, the effect of the pre-growth annealing step was investigated.

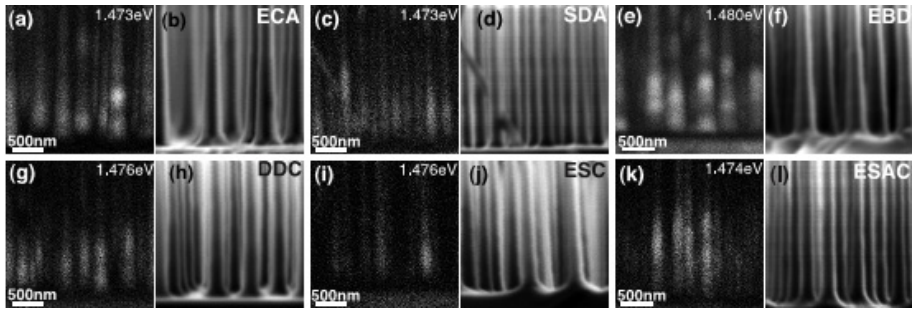

Figure 5.5: CL emissions of GaAs nanowires grown including in situ annealing step*. CL images on the left and corresponding SEM images on the right. (a), (b) ECA, (c), (d) SDA, (e), (f) EBD, (g), (h) DDC, (i),(j) ESC and (k), (l) ESAC [from ref. [26] with permission].*

Only nanowires grown at 480 °C show enough emission intensity to interpret the results. In the following, only those are mentioned here.

In general, the emission spectra of all samples are highly similar both concerning peak position and line shape. It arises, that the *in situ* annealing step plays an important role for the optical properties. Nanowires grown from different particle types had very similar emission, if an annealing step has been included before growth (Fig. 5.5). Only nanowires grown from aerosol spark-discharge particles show severe bleaching.

When growth is performed without annealing step, there is a larger variation in emission between the samples (Fig. 5.6). Nanowires grown from aerosol particles (both ECA and SDA) and EBD particles do not show significant differences from their counterparts including the annealing step. Nanowires grown from colloidal particles, however, exhibit significantly weaker emission without annealing step. Nanowires grown from DDC particles have the weakest emission, electrospraying improves the performance. ESAC particles lead to nanowires with stronger emission, but still weaker than of nanowires including annealing step. These results give evidence to incorporation of carbon remnants from the preparation into the nanowires, thereby influencing their optical properties. Surprisingly, nanowires grown from EDB particles seem not to be affect by remnants, even though the process involves numerous chemicals. Apparently, those are more volatile and evaporate, before the growth temperature is reached. The amount of remnants is significantly reduced for colloidal particles by electrospray deposition and in particular by annealing those particles before deposition. The fact, that ESC and ESAC particles still result in weaker emission, shows, that PLL as well as remnants from the colloidal solution (ligands and stabilisators) incorporate into the nanowires. The annealing step as applied in the experiments (650 °C for 6 min), however, seems to be sufficient to remove the remnants and lead to similar optical properties for nanowires grown from particles with different cleanliness. The severe bleaching of nanowires seeded by SDA particles is not fully understood.

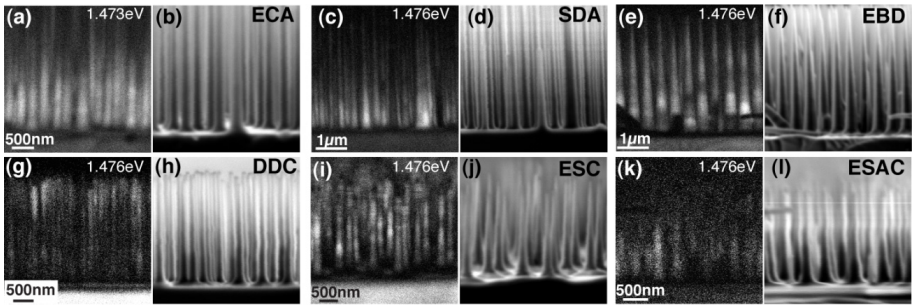

Figure 5.6: CL emissions of GaAs nanowires grown without in situ annealing step.
CL images on the left and corresponding SEM images on the right. (a), (b) ECA, (c), (d) SDA, (e), (f) EBD, (g), (h) DDC, (i),(j) ESC and (k), (l) ESAC [from [26] with permission].

It might be possible, that carbon or carbon compounds are incorporated into the particles during generation due to plastic parts in the spark discharge chamber. Palladium particles generated in the same system contained major amounts of carbon and carbon compounds [148]. Since the carbon is incorporated in the particles in contrast to colloidal particles, where carbon containing remnants cover the surface, the effect on the optical properties is different and cannot be improved by the *in situ* annealing step.

These observations lead to the conclusion, that results from different groups using different particle preparation methods can actually be compared. Differences in growth characteristics and crystal structure occur rather due to the influence of different designs of growth systems or cleaning procedures than to different particle types. Both, the investigation on the growth properties and the optical properties show the importance and the influence of the annealing step, which is neglected in many cases.

5.3 Alternative Seed Particle Materials

Gold has a major disadvantage, it is not compatible with existing silicon technology, since it may cause deep traps for carriers in the bandgap of semiconductors [149]. Au atoms from the seed particle have been found in nanowires with concentrations up to 10^{18} cm^{-3} [150-152] (which is higher than extrapolations from bulk would suggest) and harm the electronic properties [153, 154]. Up till now, it seems, that the influence of Au is still negligible compared to the negative impact of surface recombinations [150]. Another disadvantage might be the high solubility of most growth species in gold. On the one hand, this enables nanowire growth; on the other hand, it can prevent sharp interfaces in heterostructures, since the particle acts as reservoir and releases remaining material over a certain time. Therefore, several researchers have been looking for alternative seed particle materials.

One promising possibility is so-called self-seeded growth [110-112], where group III metals serve as seed particle material, for example Ga droplets for GaAs nanowire growth. This method avoids any contamination with foreign atoms. It is, however, quite challenging to get complete control over size, aspect ratios, and crystal phases, and to form arbitrary heterostructures [111]. It appears, that at least until now, that the growth is very specific to materials and growth methods, for example, reports on self-seeded GaAs NW exists only for MBE to our knowledge. In recent years, however, research groups have come very far, and highly controlled structures concerning yield, dimension control [155], and crystal structure [156] have been reported. Our group is not very active in this field at the moment, since many other groups are well established in the area.

We chose therefore another way by looking for alternative "foreign" seed materials. We believe that they hold some advantages concerning independency of size control and growth parameters and heterostructure formation. Si and Ge nanowires have been grown with the help of a number of metals including Cu, Al, Ti, Ni [19]. In many cases it was possible to achieve sharper interfaces in heterostructures than with Au particles [88]. This is due to a higher eutectic temperature of these material combinations, leading to growth from a solid particle and a limited solubility. Some years ago, III/V nanowires have been grown from Fe [114], Mn [116, 157], Ag [158] and Ni [159, 160]. These nanowires were, however, not vertically aligned to the substrate. In recent years, this was obtained for Pd seeded InAs nanowires [115, 161, 162], for Ag seeded InSb nanowires [117] and for Cu seeded InP nanowires [II, III], as discussed in the next section.

5.4 Cu-seeded Nanowire Growth

Copper was chosen as model system, since it has a lot in common with gold, but has several different properties at the same time. This knowledge will help us to map the essential properties for seed materials. Cu is also a noble metal and in the same group of the periodic system. It is ductile, has the same crystal structure, almost the same melting temperature, and is expected to have – unfortunately – similarly severe electronic properties for the integration with silicon technology; although it seems to have a less severe effect to Si solar cells [163]. In the face of large-scale production, Cu can be the material of choice, since it is less expensive than Au. There are certain distinct differences between the two metals: Cu is not inert, interacts differently with In, i.e. In has a lower solubility in Cu and the eutectic temperature is higher, and it has a different surface energy.

InP nanowires were grown from Cu seed particles formed by annealing of a thin Cu film [II, III]. The influence of temperature at a V/III ratio of 940 [II], and of molar fractions at 350 °C [III] was investigated. The V/III ratio of 940 was chosen for the temperature study, since there the highest yield of vertically-aligned nanowires in <111>B direction could be achieved. For the same reason we chose 350 °C as standard temperature for the study on molar fractions. Experimental details can be found in papers II and III, respectively.

5.4.1 Growth of Cu seeded InP nanowires dependent on temperature

In Figure 5.7, SEM micrographs show the growth of InP nanowires in the temperature range of 310 °C to 400 °C. The temperature range, where InP nanowires successfully can be grown from Cu seeds, is quite limited to 340 °C to 370 °C and narrow compared to InP nanowire growth from Au particles. Beyond this range the fraction of epitaxial nanowires decreases considerably. Below 340 °C, nucleation and growth might just be too slow to lead to nanowire structures in reasonable time. Above 390 °C we cannot observe any growth of nanowires.

The diameters of the nanowires range from 10 to 100 nm due to preparation of the seed particles from thin films. In this case, the fabrication method is very useful, since it provides a wide range of diameters, so that the dependence of the growth behavior on the diameter can easily be studied.

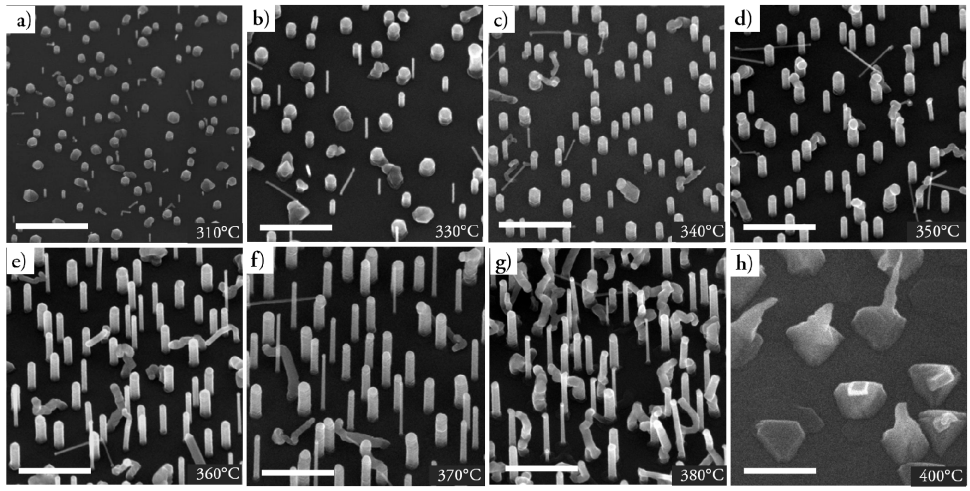

Figure 5.7: SEM micrographs of InP nanowires grown from Cu seed particles *at growth temperatures of a) 310, b) 340 d) 350, e) 360, f) 370, g) 380, and h) 400 °C; scale bars 500 nm, tilt 30°.From [II].*

The length of the nanowires is inversely dependent on the diameter for small diameter and then independent for diameters larger than about 50 nm, as described by Dubrovskii and Sibirev [164]. Both very thin and very thick nanowires have a tendency to kink. Thin nanowires kink mostly directly from the beginning and grow straight afterwards in the new direction, while thicker nanowires either grow curly or start vertically-aligned and kink later. Those nanowires which grow epitaxially along <111>B direction have a hexagonal cross section and {112} oriented sidewalls with alternating {111} A and B micro facets. The nanowires exhibit a zinc blende (ZB) crystal structure with random stacking faults and twin planes for the investigated temperatures 350 °C and 370 °C according to HR-TEM (Fig. 5.8). This is in agreement with crystal structure of Au seeded InP nanowires grown below 380 °C [40]. It seems that the change of seed material does not have an influence on the crystal structure - at least at our conditions.

The particles on top of the nanowires are strongly facetted. At 350 °C and below the particles have the form of a hexagonal pyramid (Fig. 5.8). At 370 °C and above the particles have an irregular shape, but still facetted. At 360 °C both shapes coexist. The particles have a composition of 64 at.% Cu and 36 at.% In as revealed by point XEDS measurements (the P content is below the detection limit of 2 at.%). In combination with diffraction patterns and atomic distances the phase of the particle is identified as a form of the η (Cu_2In) phase, which has a NiAs basic structure.

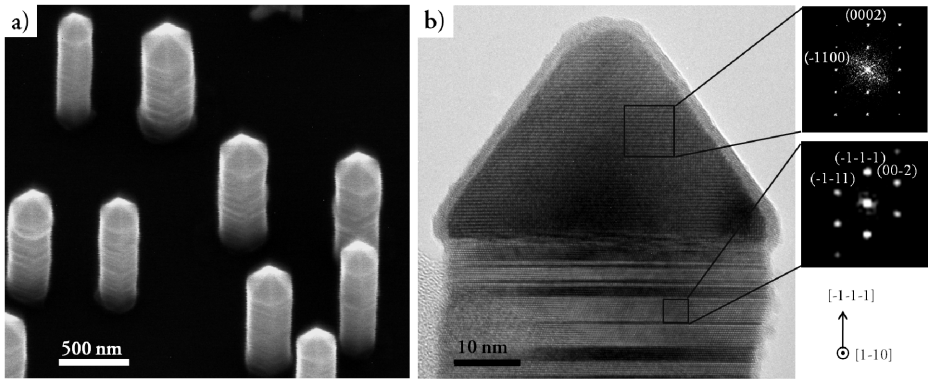

Figure 5.8: Facetted particles *on InP nanowire grown at 350 °C a) SEM micrograph, hexagonal pyramids are visible on top of the NWs, tilt 30°; b) HR-TEM micrograph of the top of an InP nanowire including FFTs of the particle and the wire. Modified from [II].*

The particle is epitaxially related to the nanowire with c-axis is parallel to the growth direction $InP\,(\bar{1}\bar{1}\bar{1})$ //$Cu_2In\,(000\bar{1})$ and $InP\,[\bar{1}\bar{1}0]$//$Cu_2In\,[1\bar{1}01]$. The lattice mismatch in the parallel densely packed planes $(\bar{1}\bar{1}\bar{1})$ in InP and $(000\bar{1})$ in Cu_2In is very small with 0.7%. Although these are room temperature and post-growth observations, there are strong indications that the nanowires grow from a solid particle. The temperature range for successful nanowire growth lies more than 300 K below the eutectic temperature according to the binary Cu-In phase diagram [7] [165]. It has been shown that liquid seed particles still can exist far below the eutectic temperature due to temperature and pressure effects [60] or due to supersaturation [61]. Still, the large undercooling, that would be required, the good epitaxial relation, and the small lattice mismatch make it reasonable to assume solid particles during growth.

[7] The application of phase diagrams on nanowire growth processes is problematic: Phase diagrams represent bulk phases occurring at thermodynamic equilibrium at atmospheric pressure. This is not given during the growth process. Nonetheless, phase diagrams can give indications for phases existing during growth. In this case for example, due to low temperatures and fast cooling times, it can be assumed that the state of the particle during growth is "frozen" due to kinetic hindering.

5.4.2 Growth of Cu seeded InP nanowires dependent on molar fractions and V/III ratios

More or less epitaxial nanowires can be grown in the range of V/III between 175 and 1860 with varying total molar fractions [III]. Higher molar fractions of PH_3 lead to enhanced growth of non-straight structures (Fig. 5.9). Although a wide range of V/III ratios and molar fractions is covered, the crystallographic morphology of vertically aligned nanowires does not vary between the different samples.

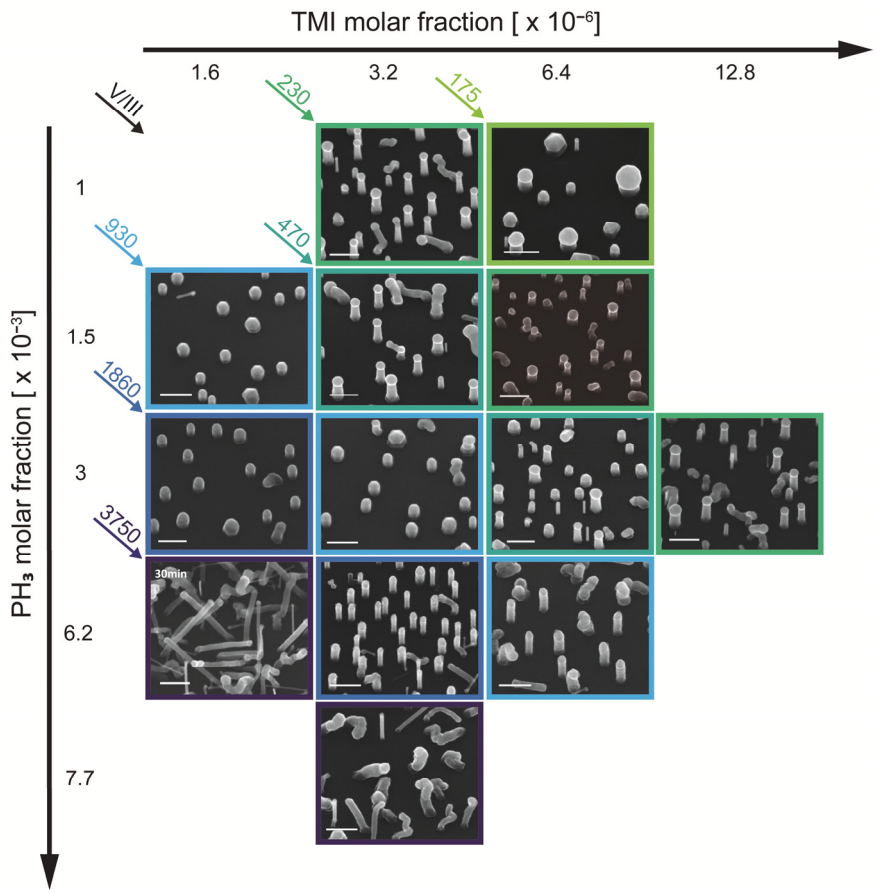

Figure 5.9: Overview of the morphology of the nanowires grown at different molar fractions and V/III ratios*. All samples are grown at 350 °C for 10 min (except marked image). Scale bar 200nm, tilt 30°. From [III].*

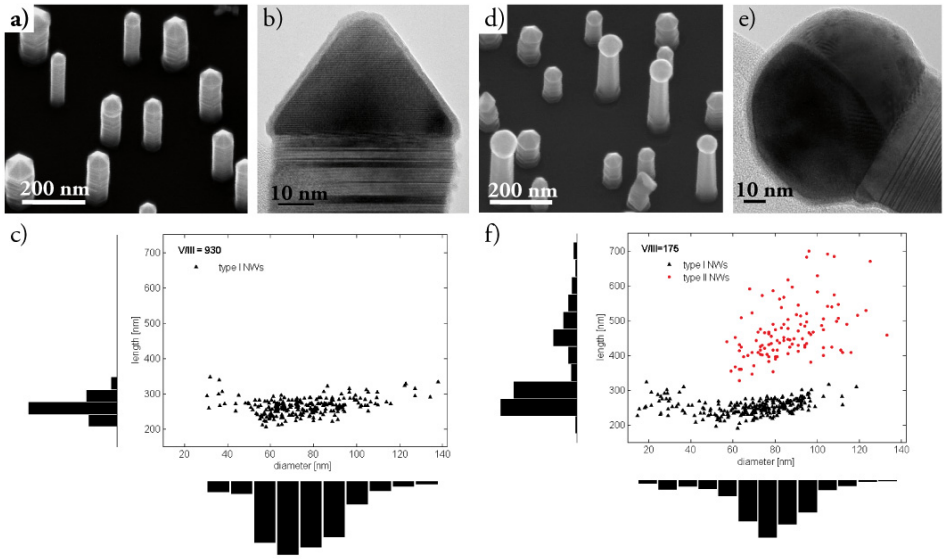

Figure 5.10: Two particle types. *a), d) SEM and b), e) HR-TEM images, c), f) and length versus diameter distribution including the histograms for nanowires grown at V/III ratios of 930 a)-c) and 175 d)-f). In d) the two types can clearly be distiguished. The length vs. diameter distribution is almost the same for type I nanowires for both V/III ratios. Growth time 30 min at 350 °C. SEM images: tilt 30°; HR-TEM images: zone axis [1-10].*

There are two types of nanowires growing in the investigated range of molar fractions and V/III ratios. The first type are nanowires described in section 5.4.1, with facetted Cu_2In particle (Fig. 5.10 a), b)), called type I further on. The second type are nanowires with an about 4 times higher growth rate compared to the first type and with a rounded, often oversized particle (Fig. 5.10 d), e)), called type II from now. Type I NWs grow under all investigated conditions, type II NWs only at V/III ratios from 470 and below. Interestingly enough, the growth rate of type I nanowires is almost the same for a V/III ratio of 930 and for 175, suggesting that their growth rate is independent of the In molar fraction at low molar fractions of PH_3.

HR-TEM and XEDS investigations show that the particles of type II nanowires consist mostly of two phases (Fig. 5.10 e)); a Cu rich part and a pure In part or shell. The amount of In in the particle increases in general with decreasing V/III ratio, but the variation within one sample is high; as the particles contain 40 at% - 90 at% In for nanowires grown at a V/III ratio of 175.

The large difference in growth rate between the two types of nanowires strongly suggests that type I nanowires grow from a solid particle, confirming the considerations in 5.4.1 and paper [II], and type II nanowires may grow from a liquid particle. Kodambaka *et al.* [60], who investigated *in situ* VLS and VSS growth of Ge

nanowires side by side, observed growth rates about seven times faster for VLS than for VSS growth. Whereas the particle phase during growth is quite obvious for type I wires, it is not for type II wires. The most probable constitution is a process similar to self-seeded growth. Two configurations of the particle are possible: A completely liquid In-rich particle or a particle with a liquid In shell and a Cu-rich, presumably Cu_2In core. The latter would be in accordance to the Cu-In binary phase diagram [165], which predicts two phases of η and an In-rich liquid at growth temperature and the post-growth compositions. Presumably, the solid Cu_2In part is situated in the middle of the particle and the liquid In-rich shell is in contact with the vapor and the growth interface. A completely liquid particle is also possible, even if the phase diagram predicts something different. During cooling in PH_3, the nanowire can continue to grow and thereby In is removed from the particle. The In concentration might therefore be higher during growth and the particle could even in accordance with the phase diagram be liquid. Other effects, such as undercooling [60] or a metastable liquid [61] could moreover play a role. In that case the phase separates during cooling, leading to the two phases observed.

The occurrence of different particle types /compositions depending on V/III ratios is not surprising in itself. Vogel *et al.*, for example, observe a similar behavior for growth of InSb nanowires from Au [107]. They found high In contents in the particle at low temperatures and low V/III ratios, and particles consisting of $AuIn_2$ at high temperatures and higher V/III ratios.

The fact that both types grow on the very same sample is, however, intriguing. The strong variation in particle composition of type II nanowires, a constant diameter over time and the observation, that all particles are facetted in the early stages of growth, leads us to a hypothesis of unsteady growth: The nanowires are seeded by Cu_2In particles first. The size of these particles determines the diameter of the NWs during the whole growth. At low V/III ratios, there might be an excess of In available, which disturbs the balance of arriving In atoms at the particle and incorporated atoms into the NW. So In accumulates in the particle, leading to a phase-separation or an In-rich liquid. In this case, the NW grows via VLS, i.e. with a higher growth rate. If the growth rate now exceeds the arrival rate, the particle is emptied from In and may turn back into solid Cu_2In. The particles may switch between the two states in a dynamic process (see Fig. 5.11) and will hence grow with varying growth rates. Depending on the individual atmosphere one or the other growth mode may be dominant for a certain NW. This may also explain the pronounced difference in length of the two NW types.

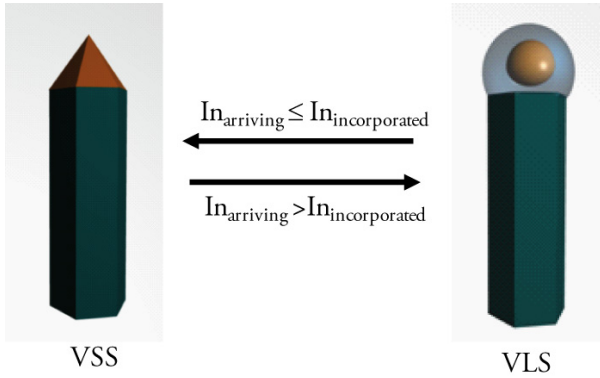

Figure 5.11: Illustration of the two growth modes and their dynamic interplay. *With low In content, the NWs grow slowly from a solid Cu_2In particle (VSS), excess In can lead to a shift to a liquid particle (VLS) and a faster growth rate.*

5.4.3 Cu-seeded InP-InAs heterostructures

A natural continuation after growing InP from Cu seed particles is to shift the group V material and test InAs. The growth conditions are expected to be similar, since mainly In forms an alloy with the Cu particle. The cracking of AsH_3 might be different, though. Unfortunately, we did not succeed growing InAs nanowires from Cu seeds on InAs substrates. We also tried to grow on {111} A substrates, since Heun *et al*. succeeded to grow InAs NWs seeded by Pd particles only on this substrate orientation [161], but without success in our case. At very low V/III ratios NWs actually grow on {111} B InAs, but XEDS analysis revealed, that the seed particles consist almost to 100% of In, i.e. these NWs grew pseudo self-seeded.

We suspected wetting problems of the Cu-In particles on the InAs substrates, which prevent that the particles are lifted up by the growing NWs, and decided therefore to grow InAs segments on top of InP stubs. Those InP stubs were grown at V/III ratio of 940 (best conditions from previous experiments) for 15 min. Afterwards various growth conditions for the growth of InAs segments were evaluated. To reduce kinking at the interface, it seems to be essential to keep both temperature and TMI molar fraction constant for both materials. Best results (in terms of highest yield of straight NWs) are achieved at temperature of 340 °C and a V/III ratio of 150 for InAs. Unfortunately, we could not find a regime, where the post-growth particles solely are of type I (facetted). This fact might imply difficulties for switching back to InP later on. Therefore the TMI flow was interrupted for 1 min after switching from AsH_3 to PH_3 with the intention to reduce the In content in the particle and restore the Cu_2In compound for most stable InP growth. Overall, growing InP segments on InAs does not pose a problem. For deeper insight into heterointerface formation and incubation time, amongst others, alternating segments of InP and InAs with varying growth times were grown in a sequence according to figure 5.12. Three segments of InP were grown, first a stem for 20 min (segment 1) and then two segments for 10 min (segments 3 and 5) alternating with InAs segments. The first InAs segment was grown for 20 min (segment 2) on the InP stem as a reference, two segments with equal growth times followed (segments 4 and 6). The time for those two segments was varied between 2 to 20 min (see Fig.5.13). About 50 (straight) NWs with different diameters and with both particle types were characterized by HR-TEM and STEM. To be able to measure the length of the segments, it was taken advantage of the contrast difference resulting from the different masses of InAs compared to InP in HAADF-STEM imaging. XEDS analysis of the particle composition and of the composition change along the nanowire completed the characterization.

***Figure 5.13: Growth sequence** of the alternating InP-InAs heterostructure.*

Despite the – for STEM analysis comparably large – number of analyzed and measured nanowires, hardly any trends could be observed. The system appears to be so complicated and influenced by so many factors that it is hard to distinguish them. Still, qualitative conclusions can be made. The reader should be aware that the following descriptions and conclusions only rely on NWs characterized by STEM, i.e. straight NWs which had been positioned on the TEM grid such that it was possible to tilt them along the zone axis [1-10].

In general, the growth rates are low, InAs grows even more slowly than InP (0.75-3.5 nm/min). As for the InP system, type I and type II post-growth particles exist. Their occurrence follows the same trend, but more clear and less overlapping compared to the results presented in 5.4.2: NWs with diameters below 50 nm are all of type I, and above 75 nm of type II. In the transition region both exist, and in some cases deviating behavior can be observed. In NWs with type I particles, InAs segment 6 is shorter than segment 4, whereas it is longer in type II NWs. Short growth times of the InAs segments are not sufficient to let segment 6 grow under the particle in many cases. The change of particle state during InAs growth has also influence on the subsequent InP segments. In type II NWs, the InP segment 5 grows faster than segment 3, whereas the growth rate is almost the same in NWs with a type I particle. Interestingly, in a transition range of diameters, where Cu_2In and In rich particles coexist, InP segment 5 is shorter than segment 3. This indicates that the dynamic change of particle composition (and state) slows down the growth, since time is required to establish steady-state. A thin and irregular InAs shell on segment 1 appears on 1/3 of the investigated NWs (Fig. 5.15-1).

The general formation of the InAs segments is very remarkable. At longer growth times (≥ 6 min) both segments 4 and 6 are visible, the InP-InAs interface is straight and sharp (Fig. 5.15-2), as well as most of the InAs-InP interfaces. For short growth times (2-8 min, even at 10 min), the projection of segment 4 is often triangular (Fig. 5.15-4), and segment 6 does not appear below the particle, but inside, mostly as a corner or islands (Fig. 5.12-5). Its interface to the InP segment under the particle is still sharp. How these structures form remains unclear, but we believe in the following hypothesis: The incubation barrier for the InAs segments is apparently very high.

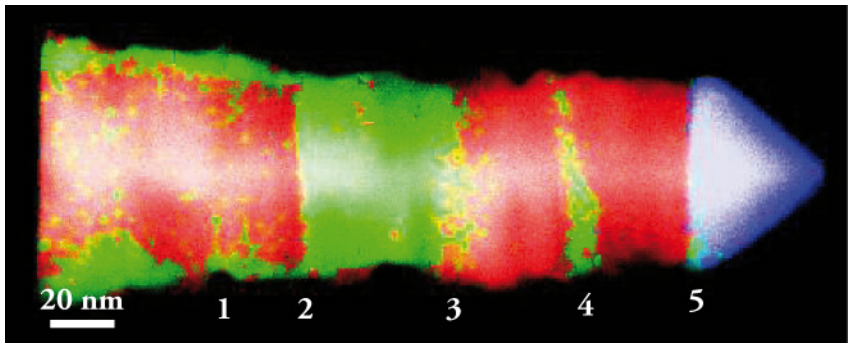

Figure 5.14: NW with examples of the different phenomena: *1. InAs overgrowth on segment 1, 2. sharp interface, 3. rough interface, 4. Segment 4 triangular, 5. InAs at corner of particle. Color coding: P red, As green, and Cu blue. Growth time for InAs segment 4 and 6: 6 min.*

Once this barrier is overcome, the amount of InAs material to be deposited is so high that it precipitates all at once as ledge nucleation and not in an ordered step-flow mechanism. For longer growth times, the segments even out and a sharp and straight interface can be retained. The high variation in segment length suggests rather a large statistical spread in nucleation time than a variation in growth rate. We believe, that InAs continues to grow more easily on InAs once the first barrier is overcome. Now it is worth to remember the wetting problems on InAs substrates, i.e. the particles wetting the surface too well, so that they do not stay as compact particles but rather as flat islands, which do not promote nanowire growth. Certainly this could be a problem even during InAs segment growth and explain the ununsual segment formation. It might be that the particle rather wets the InAs completely than to minimize the contact area. So the InAs segments stay "inside" the particle until the deformation of the particle is too large and it is energetically favorable to dewet the InAs segment (at least partly). Therefore, short InAs segments appear inside the particle and longer ones are visible under it.

The most interesting feature might be, that NWs with diameters below 30 nm exhibit 4H structure in the InAs segments 2 (Fig. 5.15). There are few reports on 4H structures in NWs [30, 42, 43, 166, 167]. The understanding of the formation of 4H structures in III/V nanowires is not yet well established. Theoretical calculations predict both lowest formation energy for 4H [168] and a narrow range of supersaturation for the formation of 4H between ZB and WZ [41]. A diameter dependence has not yet been established. It could be possible, that small particles provide a composition which leads to a supersaturation necessary for the formation of 4H. Another speculation could be, that in interaction with the Cu particle the surfaces of 4H are energetically favorable compared to both WZ and ZB.

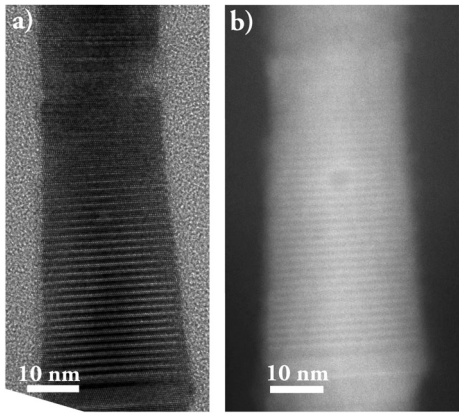

Figure 5.15: 4H structure in InAs segments *for NWs with diameters below 30 nm. a) HR-TEM image, b) HAADF-STEM image. Zone axis [1-10]*

We also have to be aware of that the nanowires are comparably short, probably below the diffusion length. Any influence of the diffusion however could not be identified. There might be a small contribution of the diffusion length, but it might be concealed by other effects. Considering the apparent complicated growth, it is quite astonishing, that a certain amount of straight NWs still could be achieved.

5.5 *In situ* Nanowire Growth

Parts of this work have been conducted at IBM T.J. Watson Research Center, Yorktown Heights, using the *in situ* UHV-TEM, which is described in 4.7.

The amazing possibility of observing nanowires while growing, comes with the question, how much the observation influences the growth, i.e. how the electron beam affects the growth. The high energy may lead to heating of the sample, beam damage and enhanced cracking of the precursors. The beam does not seem to have an effect on the growth rate, as comparisons of nanowires grown in exposed areas and those grown in unexposed areas have shown. A slight increase in temperature should not enhance the growth rate dramatically, and the change would be anyway within error margins [85]. The beam enhances, however, the growth on the sidewalls, probably due to enhanced cracking of the precursors or by removal of oxide layers (in the case of *ex situ* pre-grown nanowires). The sample geometry may also be problematic, since the growth may be dominated by edge effects. Another source of uncertainties is the indirect method of heating of the sample by sending current through the sample and calibration of power values before and/or after growth by a pyrometer. The resistance of the sample may change during growth due to changing contacts or incorporation of dopants (if GaP is grown), which makes exact temperature control almost impossible. In practice, the temperature is often estimated by heating up the sample and assuming the melting temperature of the particle as eutectic temperature.

Despite these considerations and a by far different pressure regime compared to MOVPE, this is the only method to understand growth in detail and it is definitely possible to transfer growth mechanisms from this system to other growth systems. A key finding for example was the observation of the oscillating facet as growth mechanism [144, 145], which would never have been concluded from post growth characteristics. The same holds for the investigation of kinking mechanism in heterostructures as described in 5.5.1 and paper [IV]. Furthermore, our *in situ* investigations lead to fundamental insights into the dependency of the instantaneous growth velocity in III/V materials depending on group III and group V supersaturation, as introduced in 5.5.2.

5.5.1 Hybrid group IV-group III/V heterostructured nanowires

Heterostructures of group IV and group III/V materials, i.e. III/Vs on Si, are difficult to realize in thin films, since steps on the nonpolar substrate may lead to anti-phase boundaries and stacking faults in the polar III/V material [135, 136]. Due to the small footprint of nanowires, this problem can be overcome in nanowires. III/V nanowires on Si substrates have often been realized [106, 169-175]. Hybrid nanowires are interesting due to their band structure and may lead to new functionalities in photonic devices, silicides and contact formation, and integration in Si-technology. An aim would be to grow quantum dots of the one material embedded in another. This is still difficult to achieve since the nanowires kink at or after the hetero interface in many cases. The kinking can be divided in two phenomenon: first, kinking directly at the interface and second, kinking later after the interface. The first occurs in material combinations or directions, where the second material does not wet the first material, leading to the formation of a compact nucleus (Fig. 5.18 a)), and prevention of step-flow growth [89]. The compact nucleus grows and pushes the seed particle off the NW, often leading not only to kinking, but to backwards growth.

The second occurs, if the material combination allows for step-flow-growth, but the kinking occurs later on, after a straight segment [IV]. This kinking is a result of diameter change after the heterojunction, since the particle changes volume and contact angle due to a different equilibrium composition. An example for this phenomenon is Si on GaP, which initially grows layer-by-layer (Fig. 5.16).

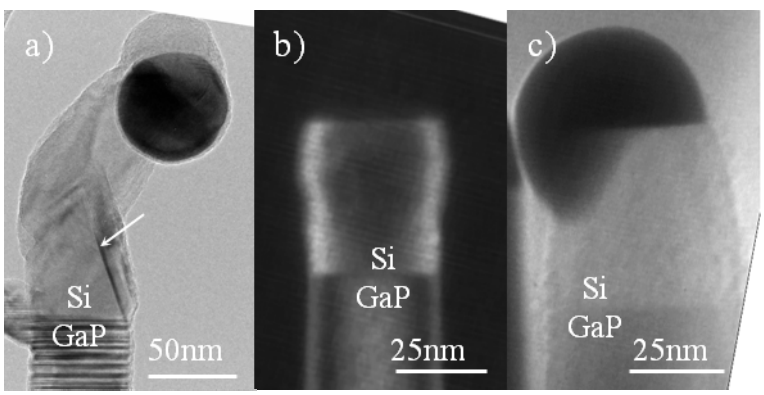

Figure 5.16: Hybrid heterostructures. *Several modes of the layer-by-layer combination GaP/Si: a) increasing diameter, formation of inclined stacking faults, b) straight nanowire and c) wetting of and inclined facet due to diameter decrease. From [IV].*

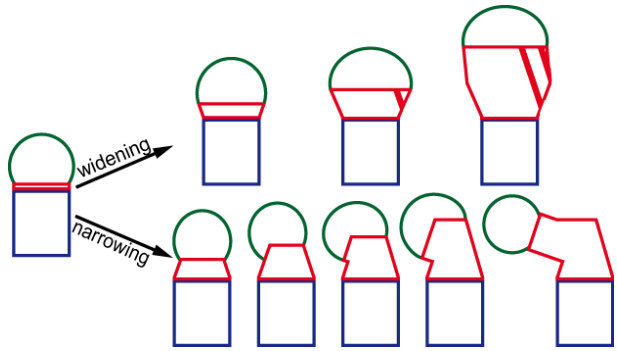

Figure 5.17: Schematic of kinking induced by diameter change after the heterojunction. *Upper row: If the NW widens due to an increasing volume of the particle, inclined stacking faults are induced. Note that the final kinking step is not shown, since no general shape is observed. Lower row: If the NW narrows due to a shinking particle, the particle wets the new inclined facets, switches between the two, until growth continues in the new direction. From [IV].*

If the diameter gradually increases after the heterojunction, which happens for example at higher temperatures, inclined stacking faults form, which later on lead to meandering kinking (Fig. 5.16 a) and Fig. 5.17 upper sequence). In the case of decreasing diameter, which is more the case at lower temperatures, inclined facets (often {111}) are formed to accommodate the shrinking diameter (Fig. 5.16 c)). The droplet will switch between the facets, if it stays on one of the new facets, the growth direction is changed and the wire will continue in the new direction with a reduced diameter without further kinking (5.17 lower sequence). A possible strategy to avoid kinking might be the control of diameter by gradually changing the growth conditions.

To realize straight combinations of materials which normally form a compact nucleus we applied the strategy of multilayers. We insert a thin layer of a material which grows layer-by-layer. Si forms a compact nucleus on GaAs (Fig. 5.18 a)), Ge grows layer-by-layer on GaAs [89], and Si can grow on Ge straight under certain conditions [88]. So it is possible to form GaAs/Ge/Si heterostructures. We realized multilayers of Si on Ge on GaAs (Fig.5.18 b) and c)), and added even an additional Ge layer on Si (Fig. 5.18 d)). Very recently, Hocevar *et al.* [133] published very similar results, where they inserted a GaAs segment into a Si NW by using GaP buffer layers. They observed similar kinking, but could overcome it by tuning the diameter and growth conditions. This shows once more, that results obtained in the *in situ* TEM are transferable to MOVPE.

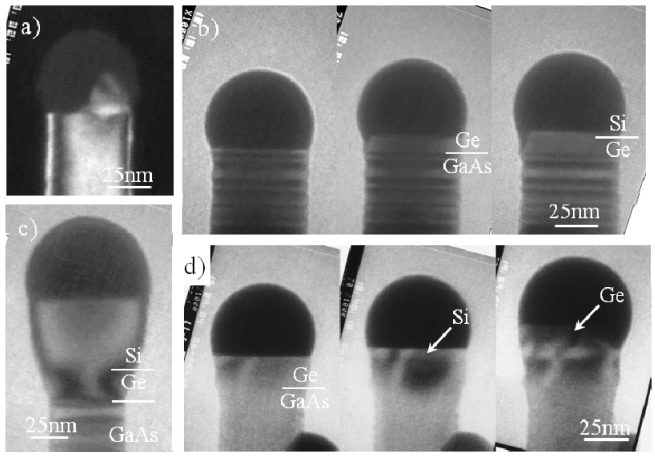

Figure 5.18: Multilayer. *a) GaAs/Si, Si forms a compact nucleus, b) sequence of growth of Si on GaAs with an intermediate Ge layer c) another GaAs/Ge/Si nanowire d) sequence of thin Ge/Si/Ge layers on GaAs. From [IV].*

5.5.2 Kinetics of *in situ* GaP nanowire growth

During my visits at the IBM Research Center, we started to extend the *in situ* investigations of NW growth from group IV materials to GaP. The contribution of two materials at the same time complicates control, but makes the observations more interesting. We investigated the growth of GaP depending on temperature, precursor pressures and V/III ratios. Such studies are standard in MOVPE and well known, but the instantaneous processes have never been observed. The growth rate dependence on temperature shows close similarity to regular MOVPE. Here, only a summary of preliminary results of our study on V/III ratios and precursor pressures is presented.

GaP NWs were pregrown by MOVPE in Lund, since the nucleation on Si is difficult and the growth rate is too low in the microscope to reach reasonable length for observation. The growth rate is measured by the frequency of oscillations, which correspond to the addition of a bilayer. As mentioned above, the temperature control is complicated by Ga diffusing into the Si substrate changed the resistance and thereby the temperature control during the experiments. In the case of GaP growth the beam obviously enhances the cracking of both TMG and PH_3.

The experimental conditions are largely determined by the achievable feeding gas pressure. An upper limit is required in order to maintain imaging conditions and to avoid poisoning of the pumping system. Further limitations arose from the required minimum TMG pressure, below which growth does not occur. The maxium total pressure, i.e. PH_3 partial pressure, lies at10^{-5} Torr. The partial pressure of TMG is limited to 5 x 10^{-8} - 5 x 10^{-6} Torr leading to V/III ratios between 20 and 1000.

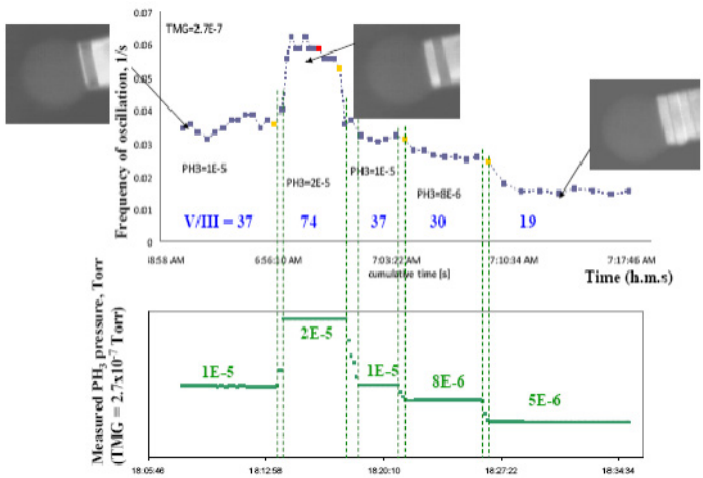

Figure 5.19: Lower V/III regime: *Growth rate dependence on PH_3 pressure. Red data point marks the formation of a twin. TMG is kept steady at 2.7 x 10^{-7} Torr, growth temperature about 450 °C.*

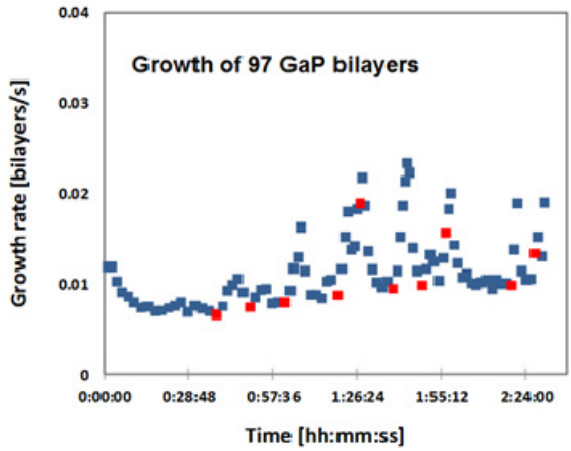

***Figure 5.20: Higher V/III ratio regime**: Growth rate over time for 97 bilayers. Red data points mark twin formation, which is followed by an increase in growth rate. PH_3 8-10 x10^{-6} Torr, TMG 5-9 x 10^{-8} Torr, Growth temperature about 450 °C.*

Within the tested range, we can identify two regimes with a transition at a V/III ratio of about 60-100: In the lower V/III ratio regime (20-60), the growth rate is strongly dependent on the PH_3 pressure, a change in TMG pressure does not influence the growth rate, i.e. the growth is limited by the arrival of P atoms. Changes in PH_3 are quickly followed by growth rate changes (Fig. 5.19). During steady-state conditions the frequency of adding bilayers is regular and only few twins are formed. The droplets, which have a large volume, i.e. contain a large fraction of Ga, and change their volume slowly dependent on the PH_3 pressure.

In the higher V/III regime (100-1000), the growth rate is irregular even under steady conditions. A dependence on PH_3 can not be observed, even the dependence on TMG pressure is only weak. The density of defects is higher compared to growth in the lower V/III ratio regime. Acceleration up to four times times can be correlated to twin formation in the ZB NW, showing a direct connection of defect formation and supersaturation. Note, that the acceleration of growth rate happens after twin formation, indicating that defects may induce a change in supersaturation. This would be very remarkable, but hard to understand.

On the basis of these observations, a kinetic model is under development, which will take into account both the influence of group III and of group IV.

6 Conclusions

The intention of the thesis was, amongst others, to investigate alternative seed particle materials for the growth III/V nanowires and contribute to a deeper understanding of the essential properties for a suitable seed material.

First of all, we could show that different particle preparation methods in the case of Au do not play an important role in matters of growth characteristics and optical properties, if a pre-growth annealing step is included.

Second, nanowire growth from Cu seed particles was successful, both for InP nanowires and even for alternating InP-InAs heterostructures. The study revealed that particle-assisted growth is more complicated than expected, and every material combination seems to hold new interesting phenomena. The results rather generated new questions than answering the ones we had. Only the expansion to many more materials may finally give an answer, but this will be an extensive project.

The results showed furthermore, how far research on nanowire growth using Au seed particles has come, if one compares quality, yield, and controllability of Au-seeded growth with Cu-seeded growth, which is only at its beginning. Two decades and hundreds of researchers are hard to beat in five years by one PhD student.

During the collaboration with IBM, we started the *in situ* TEM growth of III/V materials, which is unique up till now. We had to learn our lessons first, but they were needed as a basis for the extremely interesting observations we finally made. The continuation of these experiments will hopefully give more insight in e.g. polytypism in III/V nanowires.

7 References

[1] C. Thelander, P. Agarwal, S. Brongersma, J. Eymery, L. F. Feiner, A. Forchel, M. Scheffler, W. Riess, B. J. Ohlsson, U. Gösele and L. Samuelson, *Nanowire-based one-dimensional electronics*, Mater. Today, 9 (2006) 28-35.

[2] Y. Li, F. Qian, J. Xiang and C. M. Lieber, *Nanowire electronic and optoelectronic devices*, Mater. Today, 9 (2006) 18-27.

[3] P. J. Pauzauskie and P. Yang, *Nanowire photonics*, Mater. Today, 9 (2006) 36-45.

[4] C. P. T. Svensson, T. Mårtensson, J. Trägårdh, C. Larsson, M. Rask, D. Hessman, L. Samuelson and J. Ohlsson, *Monolithic GaAs/InGaP nanowire light emitting diodes on silicon*, Nanotechnology, 19 (2008) 6.

[5] B. Tian, T. J. Kempa and C. M. Lieber, *Single nanowire photovoltaics*, Chem. Soc. Rev., 38 (2009) 16-24.

[6] F. Patolsky, G. F. Zheng and C. M. Lieber, *Nanowire-based biosensors*, Anal. Chem., 78 (2006) 4260-4269.

[7] H. K. Hardy, *The Filamentary Growth of Metals*, Progress in Metal Physics, 6 (1956) 45-73.

[8] *Growth and Perfection of Crystals*, Chapman & Hall, 1958.

[9] R. S. Wagner and W. C. Ellis, *Vapor-Liquid-Solid Mechanism of Single Crystal Growth*, Appl. Phys. Lett., 4 (1964) 89-90.

[10] R. L. Barns and W. C. Ellis, *Gallium Arsenide + Gallium Phosphide Whisker Crystals grown by Vapor-Liquid-Solid Mechanism*, Jom-Journal of Metals, 16 (1964) 761.

[11] R. L. Barns and W. C. Ellis, *Whisker Crystals of Gallium Arsenide and Gallium Phosphide grown by Vapor-Liquid-Solid Mechanism*, J. Appl. Phys., 36 (1965) 2296-2301.

[12] J. J. Nickl and W. Just, *Growth of Gallium Arsenide Crystals using VLS Mechanisms*, J. Cryst. Growth, 11 (1971) 11-20.

[13] H. Morkoc, R. Stamberg and E. Krikorian, *Whisker Growth during Epitaxy of GaAs by Molecular-beam Epitaxy*, Japanese Journal of Applied Physics Part 2-Letters, 21 (1982) L230-L232.

[14] E. I. Givargizov, *Highly Anisotropic Crystals*, D. Reidel, Doordrecht, 1987.

[15] K. Hiruma, T. Katsuyama, K. Ogawa, M. Koguchi, H. Kakibayashi and G. P. Morgan, *Quantum Size Microcrystals grown using Organometallic Vapor-Phase Epitaxy*, Appl. Phys. Lett., 59 (1991) 431-433.

[16] M. Yazawa, M. Koguchi, A. Muto, M. Ozawa and K. Hiruma, *Effect of one Monolayer of Surface Gold Atoms on the Epitaxial-Growth of InAs Nanowhiskers*, Appl. Phys. Lett., 61 (1992) 2051-2053.

[17] L. Samuelson, C. Thelander, M. T. Bjork, M. Borgström, K. Deppert, K. A. Dick, A. E. Hansen, T. Mårtensson, N. Panev, A. I. Persson, W. Seifert, N. Sköld, M. W. Larsson and L. R. Wallenberg, *Semiconductor nanowires for 0D and 1D physics and applications*, Physica E-Low-Dimensional Systems & Nanostructures, 25 (2004) 313-318.

[18] V. Schmidt, J. V. Wittemann and U. Gösele, *Growth, Thermodynamics, and Electrical Properties of Silicon Nanowires*, Chem. Rev., 110 (2010) 361-388.

[19] J. L. Lensch-Falk, E. R. Hemesath, D. E. Perea and L. J. Lauhon, *Alternative catalysts for VSS growth of silicon and germanium nanowires*, J. Mater. Chem., 19 (2009) 849-857.

[20] F. M. Ross, C. Y. Wen, S. Kodambaka, B. A. Wacaser, M. C. Reuter and E. A. Stach, *The growth and characterization of Si and Ge nanowires grown from reactive metal catalysts*, Philosophical Magazine, 90 (2010) 2807-2816.

[21] K. A. Dick, *A review of nanowire growth promoted by alloys and non-alloying elements with emphasis on Au-assisted III-V nanowires*, Prog. Cryst. Growth Charact. Mater., 54 (2008) 138-173.

[22] P. Prete and N. Lovergine, *MOVPE Self-Assembly and Physical Properties of Free-Standing III-V Nanowires*, in: P. Prete (Ed.), Nanowires, InTech, 2010, pp. 51-78.

[23] C. N. R. Rao, F. L. Deepak, G. Gundiah and A. Govindaraj, *Inorganic nanowires*, Prog. Solid State Chem., 31 (2003) 5-147.

[24] Z. L. Wang, *Zinc oxide nanostructures: growth, properties and applications*, Journal of Physics-Condensed Matter, 16 (2004) R829-R858.

[25] B. J. Ohlsson, M. T. Björk, M. H. Magnusson, K. Deppert, L. Samuelson and L. R. Wallenberg, *Size-, shape-, and position-controlled GaAs nano-whiskers*, Appl. Phys. Lett., 79 (2001) 3335-3337.

[26] A. Gustafsson, K. Hillerich, M. E. Messing, K. Storm, K. A. Dick, K. Deppert and J. Bolinsson, *A cathodoluminescence study of the influence of the seed particle preparation method on the optical properties of GaAs nanowires*, Nanotechnology, 23 (2012) 9.

[27] C. Y. Wen, J. Tersoff, K. Hillerich, M. C. Reuter, J. H. Park, S. Kodambaka, E. A. Stach and F. M. Ross, *Periodically Changing Morphology of the Growth Interface in Si, Ge, and GaP Nanowires*, Phys. Rev. Lett., 107 (2011) 025503.

[28] W. Borchardt-Ott, *Crystallography - In Introduction*, Springer Berlin Heidelberg, 2012, pp. 9-21.

[29] P. Caroff, J. Bolinsson and J. Johansson, *Crystal Phases in III-V Nanowires: From Random Toward Engineered Polytypism*, IEEE J. Sel. Top. Quantum Electron., 17 (2011) 829-846.

[30] D. L. Dheeraj, G. Patriarche, H. L. Zhou, T. B. Hoang, A. F. Moses, S. Gronsberg, A. T. J. van Helvoort, B. O. Fimland and H. Weman, *Growth and Characterization of Wurtzite GaAs Nanowires with Defect-Free Zinc Blende GaAsSb Inserts*, Nano Lett., 8 (2008) 4459-4463.

[31] K. A. Dick, C. Thelander, L. Samuelson and P. Caroff, *Crystal Phase Engineering in Single InAs Nanowires*, Nano Lett., 10 (2010) 3494-3499.

[32] P. K. Mohseni and R. R. LaPierre, *A growth interruption technique for stacking fault-free nanowire superlattices*, Nanotechnology, 20 (2009) 025610.

[33] J. A. Venables, *Introduction to Surface and Thin Film Processes*, Cambridge University Press, New York, 2000, pp. 9-19.

[34] J. A. Venables, *Introduction to Surface and Thin Film Processes*, Cambridge University Press, New York, 2000, pp. 144-149.

[35] J. Johansson, L. S. Karlsson, K. A. Dick, J. Bolinsson, B. A. Wacaser, K. Deppert and L. Samuelson, *Effects of Supersaturation on the Crystal Structure of Gold Seeded III-V Nanowires*, Crystal Growth & Design, 9 (2009) 766-773.

[36] J. A. Venables, *Introduction to Surface and Thin Film Processes*, Cambridge University Press, New York, 2000, pp. 149-157.

[37] D. L. Smith, *Thim-film deposition*, McGraw-Hill, 1995, pp. 355-358.

[38] I. V. Markov, *Crystal growth for beginners*, World Scientific Publishing, 2003, pp. 191.

[39] Y. Imry, *Introduction to mesoscopic physics*, 2nd ed. Oxford University Press, Oxford, 2002.

[40] K. A. Dick, P. Caroff, J. Bolinsson, M. E. Messing, J. Johansson, K. Deppert, L. R. Wallenberg and L. Samuelson, *Control of III-V nanowire crystal structure by growth parameter tuning*, Semicond. Sci. Technol., 25 (2010) 11.

[41] J. Johansson, J. Bolinsson, M. Ek, P. Caroff and K. A. Dick, *Combinatorial Approaches to Understanding Polytypism in III/V Nanowires*, ACS Nano, 6 (2012) 6142-6149.

[42] B. Mandl, K. A. Dick, D. Kriegner, M. Keplinger, G. Bauer, J. Stangl and K. Deppert, *Crystal structure control in Au-free self-seeded InSb wire growth*, Nanotechnology, 22 (2011) 145603.

[43] J. P. Boulanger and R. R. LaPierre, *Polytype formation in GaAs/GaP axial nanowire heterostructures*, J. Cryst. Growth, 332 (2011) 21-26.

[44] S. O. Mariager, C. B. Sorensen, M. Aagesen, J. Nygard, R. Feidenhans'l and P. R. Willmott, *Facet structure of GaAs nanowires grown by molecular beam epitaxy*, Appl. Phys. Lett., 91 (2007).

[45] H. Zhang, F. Huang, B. Gilbert and J. F. Banfield, *Molecular Dynamics Simulations, Thermodynamic Analysis, and Experimental Study of Phase Stability of Zinc Sulfide Nanoparticles,* The Journal of Physical Chemistry B, 107 (2003) 13051-13060.

[46] V. G. Dubrovskii and N. V. Sibirev, *Growth thermodynamics of nanowires and its application to polytypism of zinc blende III-V nanowires*, Physical Review B, 77 (2008) 035414.

[47] F. Glas, J. C. Harmand and G. Patriarche, *Why does wurtzite form in nanowires of III-V zinc blende semiconductors?*, Phys. Rev. Lett., 99 (2007).

[48] T. Akiyama, K. Sano, K. Nakamura and T. Ito, *An empirical potential approach to wurtzite-zinc-blende polytypism in group III-V semiconductor nanowires*, Jpn. J. Appl. Phys. Part 2 - Lett. Express Lett., 45 (2006) L275-L278.

[49] J. Johansson, K. A. Dick, P. Caroff, M. E. Messing, J. Bolinsson, K. Deppert and L. Samuelson, *Diameter Dependence of the Wurtzite-Zinc Blende Transition in InAs Nanowires*, Journal of Physical Chemistry C, 114 (2010) 3837-3842.

[50] T. Yamashita, K. Sano, T. Akiyama, K. Nakamura and T. Ito, *Theoretical investigations on the formation of wurtzite segments in group III-V semiconductor nanowires*, Appl. Surf. Sci., 254 (2008) 7668-7671.

[51] P. Caroff, K. A. Dick, J. Johansson, M. E. Messing, K. Deppert and L. Samuelson, *Controlled polytypic and twin-plane superlattices in III-V nanowires*, Nature Nanotechnology, 4 (2009) 50-55.

[52] H. J. Joyce, J. Wong-Leung, Q. Gao, H. H. Tan and C. Jagadish, *Phase Perfection in Zinc Blende and Wurtzite III-V Nanowires Using Basic Growth Parameters*, Nano Lett., 10 (2010) 908-915.

[53] L. E. Fröberg, W. Seifert and J. Johansson, *Diameter-dependent growth rate of InAs nanowires*, Physical Review B, 76 (2007).

[54] V. G. Dubrovskii, N. V. Sibirev, G. E. Cirlin, I. P. Soshnikov, W. H. Chen, R. Larde, E. Cadel, P. Pareige, T. Xu, B. Grandidier, J. P. Nys, D. Stievenard, M. Moewe, L. C. Chuang and C. Chang-Hasnain, *Gibbs-Thomson and diffusion-induced contributions to the growth rate of Si, InP, and GaAs nanowires*, Physical Review B, 79 (2009).

[55] K. Dick, T. Dhanasekaran, Z. Y. Zhang and D. Meisel, *Size-dependent melting of silica-encapsulated gold nanoparticles*, J. Am. Chem. Soc., 124 (2002) 2312-2317.

[56] G. Ouyang, X. Tan, C. X. Wang and G. W. Yang, *Solid solubility limit in alloying nanoparticles*, Nanotechnology, 17 (2006) 4257-4262.

[57] R. Vallee, M. Wautelet, J. P. Dauchot and M. Hecq, *Size and segregation effects on the phase diagrams of nanoparticles of binary systems*, Nanotechnology, 12 (2001) 68-74.

[58] U. Tartaglino, T. Zykova-Timan, F. Ercolessi and E. Tosatti, *Melting and nonmelting of solid surfaces and nanosystems*, Phys. Rep.-Rev. Sec. Phys. Lett., 411 (2005) 291-321.

[59] A. I. Persson, M. W. Larsson, S. Stenström, B. J. Ohlsson, L. Samuelson and L. R. Wallenberg, *Solid-phase diffusion mechanism for GaAs nanowire growth*, Nature Materials, 3 (2004) 677-681.

[60] S. Kodambaka, J. Tersoff, M. C. Reuter and F. M. Ross, *Germanium nanowire growth below the eutectic temperature*, Science, 316 (2007) 729-732.

[61] A. D. Gamalski, J. Tersoff, R. Sharma, C. Ducati and S. Hofmann, *Formation of metastable liquid catalyst during subeutectic growth of germanium nanowires*, Nano Lett., 10 (2010) 2972-2976.

[62] G. B. Stringfellow, *Organometallic Vapor-Phase Epitaxy*, 2nd ed. Academic Press, 1999.

[63] D. L. Smith, *Thim-film deposition*, McGraw-Hill, 1995, pp. 317-330

[64] G. B. Stringfellow, *Organometallic Vapor-Phase Epitaxy*, Academic Press, 1999, pp. 225-281.

[65] C. A. Larsen, N. I. Buchan and G. B. Stringfellow, *Mass-spectrometric studies of phosphine pyrolysis and OMVPE growth of InP*, J. Cryst. Growth, 85 (1987) 148-153.

[66] G. B. Stringfellow, *Organometallic Vapor-Phase Epitaxy*, Academic Press, 1999, pp. 151-210.

[67] C. G. Granqvist and R. A. Buhrman, *Size distributions for supported metal catalysts: Coalescence growth versus ostwald ripening*, J. Catal., 42 (1976) 477-479.

[68] K. Hiruma, K. Haraguchi, M. Yazawa, Y. Madokoro and T. Katsuyama, *Nanometre-sized GaAs wires grown by organo-metallic vapour-phase epitaxy*, Nanotechnology, 17 (2006) S369-S375.

[69] M. C. Plante, J. Garrett, S. C. Ghosh, P. Kruse, H. Schriemer, T. Hall and R. R. LaPierre, *The formation of supported monodisperse Au nanoparticles by UV/ozone oxidation process*, Appl. Surf. Sci., 253 (2006) 2348-2354.

[70] T. Mårtensson, M. Borgström, W. Seifert, B. J. Ohlsson and L. Samuelson, *Fabrication of individually seeded nanowire arrays by vapour-liquid-solid growth*, Nanotechnology, 14 (2003) 1255-1258.

[71] G. Schmid, *Large Clusters and Colloids - Metals in the Embryonic State*, Chem. Rev., 92 (1992) 1709-1727.

[72] A. I. Hochbaum, R. Fan, R. R. He and P. D. Yang, *Controlled growth of Si nanowire arrays for device integration*, Nano Lett., 5 (2005) 457-460.

[73] P. H. M. Böttger, Z. Bi, D. Adolph, K. A. Dick, L. S. Karlsson, M. N. A. Karlsson, B. A. Wacaser and K. Deppert, *Electrospraying of colloidal nanoparticles for seeding of nanostructure growth*, Nanotechnology, 18 (2007) 6.

[74] M. H. Magnusson, K. Deppert, J.-O. Malm, J.-O. Bovin and L. Samuelson, *Gold nanoparticles: Production, reshaping, and thermal charging*, J. Nanopart. Res., 1 (1999) 243-251.

[75] M. E. Messing, K. A. Dick, L. R. Wallenberg and K. Deppert, *Generation of size-selected gold nanoparticles by spark discharge – for growth of epitaxial nanowires*, Gold Bulletin, 42 (2009) 20-26.

[76] D. B. Williams and C. B. Carter, *Basics*, *Transmission Electron Microscopy*, Springer, 2009, pp. 3-20.

[77] D. B. Williams and C. B. Carter, *Basics*, *Transmission Electron Microscopy*, Springer, 2009, pp. 67-84.

[78] D. B. Williams and C. B. Carter, *Basics*, *Transmission Electron Microscopy*, Springer, 2009, pp. 85-104.

[79] D. B. Williams and C. B. Carter, *Diffraction*, *Transmission Electron Microscopy*, Springer, 2009, pp. 177-213.

[80] W. Borchardt-Ott, *Crystallography - An Introduction*, Springer Berlin Heidelberg, 2012, pp. 30ff.

[81] D. B. Williams and C. B. Carter, *Imaging*, *Transmission Electron Microscopy*, Springer, 2009, pp. 349-366.

[82] D. B. Williams and C. B. Carter, *Imaging*, *Transmission Electron Microscopy*, Springer, 2009, pp. 439-481.

[83] D. B. Williams and C. B. Carter, *Basics*, *Transmission Electron Microscopy*, Springer, 2009, pp. 144-146.

[84] D. B. Williams and C. B. Carter, *Spectroscopy*, *Transmission Electron Microscopy*, Springer, 2009, pp. 553-619.

[85] F. M. Ross, *Controlling nanowire structures through real time growth studies*, Rep. Prog. Phys., 73 (2010) 114501.

[86] M. T. Björk, B. J. Ohlsson, T. Sass, A. I. Persson, C. Thelander, M. H. Magnusson, K. Deppert, L. R. Wallenberg and L. Samuelson, *One-dimensional Steeplechase for Electrons Realized*, Nano Lett., 2 (2002) 87-89.

[87] Y. Wu, J. Xiang, C. Yang, W. Lu and C. M. Lieber, *Single-crystal metallic nanowires and metal/semiconductor nanowire heterostructures,* Nature, 430 (2004) 61-65.

[88] C. Y. Wen, M. C. Reuter, J. Bruley, J. Tersoff, S. Kodambaka, E. A. Stach and F. M. Ross, *Formation of compositionally abrupt axial heterojunctions in silicon-germanium nanowires*, Science, 326 (2009) 1247-1250.

[89] K. A. Dick, S. Kodambaka, M. C. Reuter, K. Deppert, L. Samuelson, W. Seifert, L. R. Wallenberg and F. M. Ross, *The morphology of axial and branched nanowire heterostructures*, Nano Lett., 7 (2007) 1817-1822.

[90] B. M. Borg, K. A. Dick, B. Ganjipour, M. E. Pistol, L. E. Wernersson and C. Thelander, *InAs/GaSb Heterostructure Nanowires for Tunnel Field-Effect Transistors*, Nano Lett., 10 (2010) 4080-4085.

[91] R. E. Algra, M. Hocevar, M. A. Verheijen, I. Zardo, G. G. W. Immink, W. J. P. van Enckevort, G. Abstreiter, L. P. Kouwenhoven, E. Vlieg and E. Bakkers, *Crystal Structure Transfer in Core/Shell Nanowires*, Nano Lett., 11 (2011) 1690-1694.

[92] L. J. Lauhon, M. S. Gudiksen, C. L. Wang and C. M. Lieber, *Epitaxial core-shell and core-multishell nanowire heterostructures*, Nature, 420 (2002) 57-61.

[93] N. Sköld, L. S. Karlsson, M. W. Larsson, M. E. Pistol, W. Seifert, J. Trägårdh and L. Samuelson, *Growth and optical properties of strained GaAs-GaxIn1-xP core-shell nanowires*, Nano Lett., 5 (2005) 1943-1947.

[94] P. Prete, F. Marzo, P. Paiano, N. Lovergine, G. Salviati, L. Lazzarini and T. Sekiguchi, *Luminescence of GaAs/AlGaAs core-shell nanowires grown by MOVPE using tertiarybutylarsine*, J. Cryst. Growth, 310 (2008) 5114-5118.

[95] J. W. W. van Tilburg, R. E. Algra, W. G. G. Immink, M. Verheijen, E. Bakkers and L. P. Kouwenhoven, *Surface passivated InAs/InP core/shell nanowires*, Semicond. Sci. Technol., 25 (2010) 024011.

[96] S. G. Ghalamestani, M. Heurlin, L.-E. Wernersson, S. Lehmann and K. A. Dick, *Growth of InAs/InP core-shell nanowires with various pure crystal structures*, Nanotechnology, 23 (2012) 285601.

[97] J. Johansson and K. A. Dick, *Recent advances in semiconductor nanowire heterostructures*, CrystEngComm, 13 (2011) 7175-7184.

[98] P. Caroff, J. Bolinsson and J. Johansson, *Crystal Phases in III-V Nanowires: From Random Toward Engineered Polytypism*, Selected Topics in Quantum Electronics, IEEE Journal of, PP (2010) 18-18.

[99] M. T. Borgström, E. Norberg, P. Wickert, H. A. Nilsson, J. Trägårdh, K. A. Dick, G. Statkute, P. Ramvall, K. Deppert and L. Samuelson, *Precursor evaluation for in situ InP nanowire doping*, Nanotechnology, 19 (2008) 445602.

[100] I. Regolin, C. Gutsche, A. Lysov, K. Blekker, Z. A. Li, M. Spasova, W. Prost and F. J. Tegude, *Axial pn-junctions formed by MOVPE using DEZn and TESn in vapor-liquid-solid grown GaAs nanowires*, J. Cryst. Growth, 315 (2011) 143-147.

[101] J. Wallentin, M. Ek, L. R. Wallenberg, L. Samuelson, K. Deppert and M. T. Borgström, *Changes in contact angle of seed particle correlated with increased zincblende formation in doped InP nanowires*, Nano Lett., 10 (2010) 4807-4812.

[102] J. Wallentin and M. T. Borgström, *Doping of semiconductor nanowires*, J. Mater. Res., 26 (2011) 2142-2156.

[103] J. Dufouleur, C. Colombo, T. Garma, B. Ketterer, E. Uccelli, M. Nicotra and A. Fontcuberta i Morral, *P-Doping Mechanisms in Catalyst-Free Gallium Arsenide Nanowires*, Nano Lett., 10 (2010) 1734-1740.

[104] T. Xu, K. A. Dick, S. Plissard, N. Thanh Hai, Y. Makoudi, M. Berthe, J.-P. Nys, X. Wallart, B. Grandidier and P. Caroff, *Faceting, composition and crystal phase evolution in III-V antimonide nanowire heterostructures revealed by combining microscopy techniques*, Nanotechnology, 23 (2012).

[105] P. Caroff, M. E. Messing, B. M. Borg, K. A. Dick, K. Deppert and L. E. Wernersson, *InSb heterostructure nanowires: MOVPE growth under extreme lattice mismatch*, Nanotechnology, 20 (2009) 495606.

[106] S. Plissard, K. A. Dick, X. Wallart and P. Caroff, *Gold-free GaAs/GaAsSb heterostructure nanowires grown on silicon*, Appl. Phys. Lett., 96 (2010) 121901.

[107] A. T. Vogel, J. de Boor, J. V. Wittemann, S. L. Mensah, P. Werner and V. Schmidt, *Fabrication of high-quality InSb nanowire arrays by chemical beam epitaxy*, Crystal Growth & Design, 11 (2011) 1896-1900.

[108] S. G. Ghalamestani, M. Ek, B. Ganjipour, C. Thelander, J. Johansson, P. Caroff and K. A. Dick, *Demonstration of Defect-Free and Composition Tunable GaxIn1-xSb Nanowires*, Nano Lett., 12 (2012) 4914-4919.

[109] D. Spirkoska, G. Abstreiter and A. F. i. Morral, *GaAs nanowires and related prismatic heterostructures*, Semicond. Sci. Technol., 24 (2009) 113001.

[110] B. Mandl, J. Stangl, E. Hilner, A. A. Zakharov, K. Hillerich, A. W. Dey, L. Samuelson, G. Bauer, K. Deppert and A. Mikkelsen, *Growth mechanism of self-catalyzed group III-V nanowires*, Nano Lett., 10 (2010) 4443-4449.

[111] A. Fontcuberta i Morral, *Gold-Free GaAs Nanowire Synthesis and Optical Properties*, IEEE J. Sel. Top. Quantum Electron., 17 (2011) 819-828.

[112] M. Mattila, T. Hakkarainen and H. Lipsanen, *Catalyst-free fabrication of InP and InP(N) nanowires by metalorganic vapor phase epitaxy*, J. Cryst. Growth, 298 (2007) 640-643.

[113] F. Martelli, S. Rubini, M. Piccin, G. Bais, F. Jabeen, S. De Franceschi, V. Grillo, E. Carlino, F. D'Acapito, F. Boscherini, S. Cabrini, M. Lazzarino, L. Businaro, F. Romanato and A. Franciosi, *Manganese-induced growth of GaAs nanowires*, Nano Lett., 6 (2006) 2130-2134.

[114] I. Regolin, V. Khorenko, W. Prost, F. J. Tegude, D. Sudfeld, J. Kastner, G. Dumpich, K. Hitzbleck and H. Wiggers, *GaAs whiskers grown by metal-organic vapor-phase epitaxy using Fe nanoparticles*, J. Appl. Phys., 101 (2007) 054318.

[115] S. Heun, B. Radha, D. Ercolani, G. U. Kulkarni, F. Rossi, V. Grillo, G. Salviati, F. Beltram and L. Sorba, *Pd-assisted growth of InAs nanowires*, Crystal Growth & Design, 10 (2010) 4197-4202.

[116] F. Jabeen, M. Piccin, L. Felisari, V. Grillo, G. Bais, S. Rubini, F. Martelli, F. d'Acapito, M. Rovezzi and F. Boscherini, *Mn-induced growth of InAs nanowires*, Journal of Vacuum Science & Technology B, 28 (2010) 478-483.

[117] A. T. Vogel, J. de Boor, M. Becker, J. V. Wittemann, S. L. Mensah, P. Werner and V. Schmidt, *Ag-assisted CBE growth of ordered InSb nanowire arrays*, Nanotechnology, 22 (2011) 015605.

[118] K. Hillerich, M. E. Messing, L. R. Wallenberg, K. Deppert and K. A. Dick, *Epitaxial InP nanowire growth from Cu seed particles*, J. Cryst. Growth, 315 (2011) 134-137.

[119] K. Ikejiri, J. Noborisaka, S. Hara, J. Motohisa and T. Fukui, *Mechanism of catalyst-free growth of GaAs nanowires by selective area MOVPE*, J. Cryst. Growth, 298 (2007) 616-619.

[120] R. Q. Zhang, Y. Lifshitz and S. T. Lee, *Oxide-Assisted Growth of Semiconducting Nanowires*, Adv. Mater., 15 (2003) 635-640.

[121] A. Mikkelsen, J. Eriksson, E. Lundgren, J. N. Andersen, J. Weissenreider and W. Seifert, *The influence of lysine on InP(001) surface ordering and nanowire growth*, Nanotechnology, 16 (2005) 2354-2359.

[122] M. J. Tambe, L. F. Allard and S. Gradecak, *Characterization of core-shell GaAs/AlGaAs nanowire heterostructures using advanced electron microscopy*, 16th International Conference on Microscopy of Semiconducting Materials, 209 (2010).

[123] D. Spirkoska, A. Fontcuberta i Morral, J. Dufouleur, Q. Xie and G. Abstreiter, *Free standing modulation doped core-shell GaAs/AlGaAs hetero-nanowires*, Physica Status Solidi-Rapid Research Letters, 5 (2011) 353-355.

[124] L. E. Fröberg, B. A. Wacaser, J. B. Wagner, S. Jeppesen, B. J. Ohlsson, K. Deppert and L. Samuelson, *Transients in the Formation of Nanowire Heterostructures*, Nano Lett., 8 (2008) 3815-3818.

[125] M. S. Gudiksen, L. J. Lauhon, J. Wang, D. C. Smith and C. M. Lieber, *Growth of nanowire superlattice structures for nanoscale photonics and electronics*, Nature, 415 (2002) 617-620.

[126] F. Jabeen, G. Patriarche, F. Glas and J. C. Harmand, *GaP/GaAs1-xPx nanowires fabricated with modulated fluxes: A step towards the realization of superlattices in a single nanowire*, J. Cryst. Growth, 323 (2011) 293-296.

[127] N. Li, T. Y. Tan and U. Gösele, *Transition region width of nanowire hetero- and pn-junctions grown using vapor-liquid-solid processes*, Appl. Phys. A-Mater. Sci. Process., 90 (2008) 591-596.

[128] T. E. Clark, P. Nimmatoori, K.-K. Lew, L. Pan, J. M. Redwing and E. C. Dickey, *Diameter dependent growth rate and interfacial abruptness in vapor-liquid-solid Si/Si(1-x)Ge(x) heterostructure nanowires*, Nano Lett., 8 (2008) 1246-1252.

[129] D. Y. Li, Y. Wu, R. Fan, P. D. Yang and A. Majumdar, *Thermal conductivity of Si/SiGe superlattice nanowires*, Appl. Phys. Lett., 83 (2003) 3186-3188.

[130] I. Regolin, D. Sudfeld, S. Luttjohann, V. Khorenko, W. Prost, J. Kastner, G. Dumpich, C. Meier, A. Lorke and F. J. Tegude, *Growth and characterisation of GaAs/InGaAs/GaAs nanowhiskers on (111) GaAs*, 13th International Conference on Metal Organic Vapor Phase Epitaxy, Journal, (Year) 607-611.

[131] K. A. Dick, J. Bolinsson, B. M. Borg and J. Johansson, *Controlling the Abruptness of Axial Heterojunctions in III-V Nanowires: Beyond the Reservoir Effect*, Nano Lett., 12 (2012) 3200-3206.

[132] M. E. Messing, J. Wong-Leung, Z. Zanolli, H. J. Joyce, H. H. Tan, Q. Gao, L. R. Wallenberg, J. Johansson and C. Jagadish, *Growth of Straight InAs-on-GaAs Nanowire Heterostructures*, Nano Lett., 11 (2011) 3899-3905.

[133] M. Hocevar, G. Immink, M. Verheijen, N. Akopian, V. Zwiller, L. Kouwenhoven and E. Bakkers, *Growth and optical properties of axial hybrid III-V/silicon nanowires*, Nat Commun, 3 (2012) 1266.

[134] M. W. Larsson, J. B. Wagner, M. Wallin, P. Håkansson, L. E. Fröberg, L. Samuelson and L. R. Wallenberg, *Strain mapping in free-standing heterostructured wurtzite InAs/InP nanowires*, Nanotechnology, 18 (2007) 8.

[135] S. F. Fang, K. Adomi, S. Iyer, H. Morkoc, H. Zabel, C. Choi and N. Otsuka, *Gallium arsenide and other compound semiconductors on silicon*, J. Appl. Phys., 68 (1990) R31-R58.

[136] H. Kawanami, *Heteroepitaxial technologies of III/V on Si*, Sol. Energy Mater. Sol. Cells, 66 (2001) 479-486.

[137] C. Thelander, T. Mårtensson, M. T. Björk, B. J. Ohlsson, M. W. Larsson, L. R. Wallenberg and L. Samuelson, *Single-electron transistors in heterostructure nanowires*, Appl. Phys. Lett., 83 (2003) 2052-2054.

[138] G. A. Bootsma and H. J. Gassen, *Quantitative Study on Growth of Silicon Whiskers from Silane and Germanium Whiskers from Germane*, J. Cryst. Growth, 10 (1971) 223.

[139] T. I. Kamins, R. S. Williams, D. P. Basile, T. Hesjedal and J. S. Harris, *Ti-catalyzed Si nanowires by chemical vapor deposition: Microscopy and growth mechanisms*, J. Appl. Phys., 89 (2001) 1008-1016.

[140] K. A. Dick, K. Deppert, T. Mårtensson, B. Mandl, L. Samuelson and W. Seifert, *Failure of the vapor-liquid-solid mechanism in Au-assisted MOVPE growth of InAs nanowires*, Nano Lett., 5 (2005) 761-764.

[141] B. A. Wacaser, K. A. Dick, J. Johansson, M. T. Borgström, K. Deppert and L. Samuelson, *Preferential Interface Nucleation: An Expansion of the VLS Growth Mechanism for Nanowires*, Adv. Mater., 21 (2009) 153-165.

[142] C. Y. Wen, J. Tersoff, M. C. Reuter, E. A. Stach and F. M. Ross, *Step-Flow Kinetics in Nanowire Growth*, Phys. Rev. Lett., 105 (2010) 4.

[143] S. Hofmann, R. Sharma, C. T. Wirth, F. Cervantes-Sodi, C. Ducati, T. Kasama, R. E. Dunin-Borkowski, J. Drucker, P. Bennett and J. Robertson, *Ledge-flow-controlled catalyst interface dynamics during Si nanowire growth*, Nature Materials, 7 (2008) 372-375.

[144] S. H. Oh, M. F. Chisholm, Y. Kauffmann, W. D. Kaplan, W. D. Luo, M. Rühle and C. Scheu, *Oscillatory Mass Transport in Vapor-Liquid-Solid Growth of Sapphire Nanowires*, Science, 330 (2010) 489-493.

[145] A. D. Gamalski, C. Ducati and S. Hofmann, *Cyclic Supersaturation and Triple Phase Boundary Dynamics in Germanium Nanowire Growth*, Journal of Physical Chemistry C, 115 (2011) 4413-4417.

[146] M. E. Messing, K. Hillerich, J. Johansson, K. Deppert and K. A. Dick, *The use of gold for fabrication of nanowire structures*, Gold Bulletin, 42 (2009) 172-181.

[147] L. V. Titova, T. B. Hoang, H. E. Jackson, L. M. Smith, J. M. Yarrison-Rice, Y. Kim, H. J. Joyce, H. H. Tan and C. Jagadish, *Temperature dependence of photoluminescence from single core-shell GaAs-AlGaAs nanowires*, Appl. Phys. Lett., 89 (2006).

[148] M. E. Messing, R. Westerström, B. O. Meuller, S. Blomberg, J. Gustafson, J. N. Andersen, E. Lundgren, R. van Rijn, O. Balmes, H. Bluhm and K. Deppert, *Generation of Pd Model Catalyst Nanoparticles by Spark Discharge*, Journal of Physical Chemistry C, 114 (2010) 9257-9263.

[149] S. D. Brotherton and J. E. Lowther, *Electron and Hole Capture at Au and Pt Centers in Silicon*, Phys. Rev. Lett., 44 (1980) 606.

[150] J. E. Allen, E. R. Hemesath, D. E. Perea, J. L. Lensch-Falk, Z. Y. Li, F. Yin, M. H. Gass, P. Wang, A. L. Bleloch, R. E. Palmer and L. J. Lauhon, *High-resolution detection of Au catalyst atoms in Si nanowires*, Nature Nanotechnology, 3 (2008) 168-173.

[151] D. E. Perea, J. E. Allen, S. J. May, B. W. Wessels, D. N. Seidman and L. J. Lauhon, *Three-dimensional nanoscale composition mapping of semiconductor nanowires*, Nano Lett., 6 (2006) 181-185.

[152] M. Bar-Sadan, J. Barthel, H. Shtrikman and L. Houben, *Direct Imaging of Single Au Atoms Within GaAs Nanowires*, Nano Lett., 12 (2012) 2352-2356.

[153] E. Koren, G. Elias, A. Boag, E. R. Hemesath, L. J. Lauhon and Y. Rosenwaks, *Direct Measurement of Individual Deep Traps in Single Silicon Nanowires*, Nano Lett., 11 (2011) 2499-2502.

[154] M. J. Tambe, S. Q. Ren and S. Gradecak, *Effects of Gold Diffusion on n-Type Doping of GaAs Nanowires*, Nano Lett., 10 (2010) 4584-4589.

[155] S. Plissard, K. A. Dick, G. Larrieu, S. Godey, A. Addad, X. Wallart and P. Caroff, *Gold-free growth of GaAs nanowires on silicon: arrays and polytypism*, Nanotechnology, 21 (2010) 385602.

[156] M. Heiss, S. Conesa-Boj, J. Ren, H.-H. Tseng, A. Gali, A. Rudolph, E. Uccelli, F. Peiro, J. Ramon Morante, D. Schuh, E. Reiger, E. Kaxiras, J. Arbiol and A. Fontcuberta i Morral, *Direct correlation of crystal structure and optical properties in wurtzite/zinc-blende GaAs nanowire heterostructures*, Physical Review B, 83 (2011).

[157] F. Martelli, S. Rubini, M. Piccin, G. Bais, F. Jabeen, S. De Franceschi, V. Grillo, M. Lazzarino, E. Carlino, N. Mahne, L. Businaro, F. Romanato and A. Franciosi, *Fabrication and characterization of Mn-catalyzed GaAs nanowires*, in: W. Jantsch and F. Schaffler (Eds.), Physics of Semiconductors, Pts a and B, Amer Inst Physics, Melville, 2007, pp. 59-60.

[158] J. Arbiol, A. Fontcuberta i Morral, S. Estrade, F. Peiro, B. Kalache, P. Roca i Cabarrocas and J. Ramon Morante, I*nfluence of the (111) twinning on the formation of diamond cubic/diamond hexagonal heterostructures in Cu-catalyzed Si nanowires*, J. Appl. Phys., 104 (2008).

[159] A. C. Ford, J. C. Ho, Z. Y. Fan, O. Ergen, V. Altoe, S. Aloni, H. Razavi and A. Javey, *Synthesis, Contact Printing, and Device Characterization of Ni-Catalyzed, Crystalline InAs Nanowires*, Nano Research, 1 (2008) 32-39.

[160] N. Han, F. Y. Wang, A. T. Hui, J. J. Hou, G. C. Shan, F. Xiu, T. F. Hung and J. C. Ho, *Facile synthesis and growth mechanism of Ni-catalyzed GaAs nanowires on non-crystalline substrates*, Nanotechnology, 22 (2011) 7.

[161] S. Heun, B. Radha, D. Ercolani, G. U. Kulkarni, F. Rossi, V. Grillo, G. Salviati, F. Beltram and L. Sorba, *Coexistence of vapor-liquid-solid and vapor-solid-solid growth modes in Pd-assisted InAs nanowires*, Small, 6 (2010) 1935-1941.

[162] H. Xu, Y. Wang, Y. Guo, Z. Liao, Q. Gao, H. H. Tan, C. Jagadish and J. Zou, *Defect-Free <110> Zinc-Blende Structured InAs Nanowires Catalyzed by Palladium*, Nano Lett., (2012).

[163] R. H. Hopkins and A. Rohatgi, *Impurity effects in silicon for high-efficiency solar-cells*, J. Cryst. Growth, 75 (1986) 67-79.

[164] V. G. Dubrovskii and N. V. Sibirev, *General form of the dependences of nanowire growth rate on the nanowire radius*, J. Cryst. Growth, 304 (2007) 504-513.

[165] P. Subramanian and D. Laughlin, *The Cu–In (Copper-Indium) system*, Journal of Phase Equilibria, 10 (1989) 554-568.

[166] K. Tomioka, J. Motohisa, S. Hara and T. Fukui, *Crystallographic structure of InAs nanowires studied by transmission electron microscopy*, Jpn. J. Appl. Phys. Part 2 - Lett. Express Lett., 46 (2007) L1102-L1104.

[167] D. Kriegner, C. Panse, B. Mandl, K. A. Dick, M. Keplinger, J. M. Persson, P. Caroff, D. Ercolani, L. Sorba, F. Bechstedt, J. Stangl and G. Bauer, *Unit Cell Structure of Crystal Polytypes in InAs and InSb Nanowires*, Nano Lett., 11 (2011) 1483-1489.

[168] V. G. Dubrovskii and N. V. Sibirev, *Growth thermodynamics of nanowires and its application to polytypism of zinc blende III-V nanowires*, Physical Review B, 77 (2008).

[169] E. P. A. M. Bakkers, M. T. Borgström and M. A. Verheijen, *Epitaxial growth of III-V nanowires on group IV substrates*, MRS Bull., 32 (2007) 117-122.

[170] L. Gao, R. L. Woo, B. Liang, M. Pozuelo, S. Prikhodko, M. Jackson, N. Goel, M. K. Hudait, D. L. Huffaker, M. S. Goorsky, S. Kodambaka and R. F. Hicks, *Self-Catalyzed Epitaxial Growth of Vertical Indium Phosphide Nanowires on Silicon*, Nano Lett., 9 (2009) 2223-2228.

[171] T. Mårtensson, C. P. T. Svensson, B. A. Wacaser, M. W. Larsson, W. Seifert, K. Deppert, A. Gustafsson, L. R. Wallenberg and L. Samuelson, *Epitaxial III-V nanowires on silicon*, Nano Lett., 4 (2004) 1987-1990.

[172] M. Mattila, T. Hakkarainen, H. Lipsanen, H. Jiang and E. I. Kauppinen, *Catalyst-free growth of In(As)P nanowires on silicon*, Appl. Phys. Lett., 89 (2006).

[173] S. G. Ghalamestani, S. Johansson, B. M. Borg, E. Lind, K. A. Dick and L.-E. Wernersson, *Uniform and position-controlled InAs nanowires on 2 '' Si substrates for transistor applications*, Nanotechnology, 23 (2012) 015302.

[174] K. Tomioka, T. Tanaka, S. Hara, K. Hiruma and T. Fukui, *III-V Nanowires on Si Substrate: Selective-Area Growth and Device Applications*, IEEE J. Sel. Top. Quantum Electron., 17 (2011) 1112-1129.

[175] E. Uccelli, J. Arbiol, C. Magen, P. Krögstrup, E. Russo-Averchi, M. Heiss, G. Mugny, F. Morier-Genoud, J. Nygard, J. R. Morante and A. Fontcuberta i Morral, *Three-Dimensional Multiple-Order Twinning of Self-Catalyzed GaAs Nanowires on Si Substrates*, Nano Lett., 11 (2011) 3827-3832.